# ABSTRACT

Title of thesis: MODELING AND OPTIMIZATION OF A PHOTOELECTROCHEMICAL SOLAR HYDROGEN CELL WITH $TiO_2$ AS A PHOTO-ANODE

Aisha Alobaid, Master of Science, 2014

Thesis directed by: Professor Raymond Adomaitis
Chemical and Biomolecular Engineering Department

A photoelectrochemical (PEC) cell model for solar hydrogen production with titanium dioxide ($TiO_2$) as a photo anode and platinum (Pt) as a cathode is developed. Despite the wide bandgap of $TiO_2$ resulting in limited photon absorption from the sun, it is still a good candidate due to its stability in liquid electrolytes and reasonable cost. In this model, the Beer-Lambert law is used in conjunction with the empirical diode equation to calculate the electron/hole pair generation rate in the photo-anode, and the external current reaching the cathode to estimate and optimize the hydrogen generation rate evolving at the cathode with $TiO_2$ and ITO thicknesses as optimization variables. The model revealed an optimal solution of $TiO_2$ thickness of 3230 nm at 400 nm ITO thickness, with optimal external current value of 26.9 $A/m^2$, a hydrogen generation rate of 1.394 $\times 10^{-4}$ $mol/(m^2s)$, and an overall cell efficiency $\eta_c$ of 3.4 %.

# MODELING AND OPTIMIZATION OF A PHOTOELECTROCHEMICAL SOLAR HYDROGEN CELL WITH $TiO_2$ AS A PHOTO-ANODE

by

Aisha A. Alobaid

Thesis submitted to the Faculty of the Graduate School of the
University of Maryland, College Park in partial fulfillment
of the requirements for the degree of
Master of Science
2014

Advisory Committee:
Professor Raymond Adomaitis, Chair
Professor Sheryl Ehrman
Dr. Chunsheng Wang

© Copyright by
Aisha A. Alobaid
2014

# Dedication

I dedicate this thesis to my beautiful mother, Maryam, who supported me with her unconditional love, continuous prayers and encouragement. And to my loving husband, Meshari, who always believed in me, and never stopped supporting me.

# Acknowledgments

I would like to express my deepest gratitude to Allah (God) who enlightened my way to complete my master's thesis.

I owe my gratitude to all the people who helped and supported me in completing my master's thesis.

First and foremost, I'd like to thank my advisor Professor Raymond Adomaitis for his support and encouragement. He guided me through all the times of research and thesis-writing, and was available every time I needed his advice. It has been a great pleasure to work with him, and I truly look forward to learning more from such an extraordinary individual for my PhD research.

I would also like to thank Kuwait University for awarding me a graduate fellowship, and giving me an opportunity to challenge and develop myself, and fulfill my dream. A special thanks to the chemical engineering department faculty for their continuous help and support.

I owe a special gratitude to my husband Meshari Alobaid who believed in me, supported me, encouraged me, and also learned how to cook in order to make our lives easier. In addition, I would like to thank all my family and specially my brothers and sisters: Fayza, Ibraheem, Fahad, Haya, Fatima, and Abdulaziz. A special thanks to my elder sister, Haya, for continuously sending me the family gathering photos and videos and keeping me close and updated despite the long distance. I also would like to express my gratitude to the rest of my family and my friends for their encouragement and support.

Last but not least, I express my deep gratitude to the most amazing person in my life, my mother Maryam who raised me to be the person I am today. Thank you for being there for me, thank you for believing in me, and thank you for being the most beautiful thing that happened to me in my life.

# Table of Contents

# List of Tables

# List of Figures

# Chapter 1: Introduction

## 1.1 Problem Statement

In this research, a PEC cell is considered with titanium dioxide ($TiO_2$) as a photoanode, platinum (Pt) as a cathode, and 1 M potassium hydroxide (KOH) solution as an electrolyte. The objective of this research is to analyze this system and the processes occurring as well as optimizing the rate of hydrogen generation at the cathode.

$TiO_2$ is typically deposited on a $SiO_2$ substrate (also known as quartz) coated with a transparent conducting oxide (TCO). Indium Tin Oxide (ITO) is one of the most common TCO used due to its high conductivity and high optical transparency owing to its high band gap. Tin dioxide ($SnO_2$) is also a common material used as a TCO; nevertheless, it has a lower band gap than ITO, which decreases the amount of photons passing to $TiO_2$ film. Figure 1.1 shows a schematic diagram of the photoanode, noting that the figure does not represent the actual thickness ratio between the layers ($SiO_2$, ITO, and $TiO_2$).

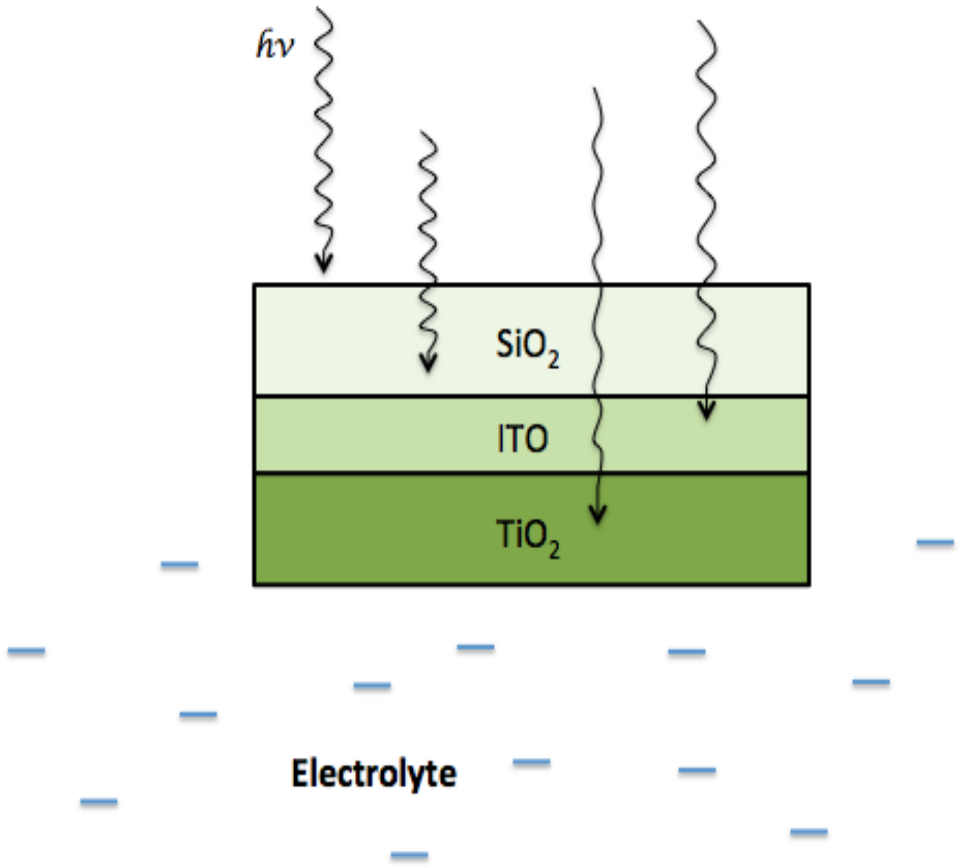


Figure 1.1: Schematic diagram of the photoanode

The thickness of $TiO_2$ determines the amount of photons absorbed governed by the absorption coefficient at different wavelengths. As more photons are absorbed, more electron/hole pairs are generated; hence, more hydrogen moles are produce. On the other hand, as the thickness of $TiO_2$ increases, the electrical resistance also increases. Thus, increasing the thickness of $TiO_2$, to a certain point, is beneficial to the performance of the PEC cell.

ITO thickness also plays an important role in the modeling and optimization of the PEC cell. The sheet resistance of ITO decreases as its thickness increases

resulting in a better electron conduction. In addition, the reflection of light between the layers can be minimized by changing the thickness of ITO (more details are provided in Section 3.1). Basic cell nonidealities are introduced in the model, such as: reflection of light between the anode layers, recombination of charge carriers in $TiO_2$, and electrical resistivities of Pt electrode, electrolyte (KOH), ITO, and $TiO_2$.

As a result, the PEC cell optimization problem is to maximize the rate of hydrogen generation, with ITO thickness ($x_1$) and $TiO_2$ thickness ($x_2$) as the optimization variables. The optimization problem is constrained by the fact that both thicknesses are non-negative, and by an upper reasonable limit of about several $\mu$m for $x_2$, and about 1 $\mu$m for $x_1$.

## 1.2 Motivation

The interest in alternative energy application is continuously increasing. The production of hydrogen via the solar water decomposition is not new to the field; however, the effort in finding the best cell conditions and components material is needed for the optimization and effective utilization of this process. Despite the enormous number of experiments and publications of the PEC cell with $TiO_2$ as a photoanode, the effect of $TiO_2$ and ITO thickness on the performance of the PEC cell has not been adequately addressed in the literature. Hence, the work done in this thesis would contribute to the field. In addition, similar methods can be used for a PEC cell with different anode material in order to test the effect of its thickness on the hydrogen generation rate.

## 1.3 Research Questions

This research is aimed to answer several important questions in the PEC cell modeling including:

- What would the effect of $TiO_2$ thickness and ITO thickness on the hydrogen production rate be, and what would the optimum photoanode film thickness be?
- What would the total electron/hole pair generation rate be as a function of film depth or thickness?
- How would introducing some nonidealities affect the overall model and the hydrogen production rate? These nonidealities may include series resistance (Pt, ITO, KOH, and $TiO_2$ electrical resistances), light reflection between the photoanode layers, and recombination of charge carriers.
- What would the characteristics of the I-V curve be?

# Chapter 2: Background and Literature Review

## 2.1 Hydrogen as the Fuel of the Future

Researchers have scrutinized the development of various hydrogen production techniques over the past two decades [1]. Due to the increasing cost of fossil fuels and the environmental impact of its direct combustion, hydrogen, as an energy carrier, is believed to be the fuel of the future [1]– [3]. Although hydrogen is not an energy source naturally available on earth in its gaseous form, it is amply available in many organic compounds such as methane, and inorganic compounds such as water [2], [4]. Several techniques have been and are still being developed to produce hydrogen from natural resources (such as wind and solar radiation). The main advantages of using such renewable energy sources to produce hydrogen are the abundance and sustainability of these sources, and that they do not pollute.

Hydrogen is a good candidate for an energy carrier, since it can be stored in liquid or gaseous forms in contrast to electricity; its transportation can be through either pipelines or tankers; it can be produced from water, which is an abundant source; it can be converted to other forms of energy efficiently; it is environmentally safe since it does not require the emission of pollutants in its production, storage, transportation and even utilization [5]. Hydrogen can also be used as a clean chem-

ical fuel with combustion energy of 142 MJ/kg producing water vapor only as a side product [5].

## 2.2 Solar Radiation

Because the focus of this thesis is on solar water splitting, we now review several important aspects of solar radiation. A blackbody is a physical object capable of absorbing all radiation falling on it, and re-emitting the radiation following Planck's Law. The sun can be treated as a blackbody; thus, the energy emitted by the sun follows Planck's Law [6] which states:

$$E_{e\lambda}(\lambda, T) = \frac{2\pi hc^2}{\lambda^5 \left[ exp\left( \frac{hc}{\lambda k_B T} \right) - 1 \right]} \tag{2.1}$$

where $E_{e\lambda}$ is the spectral irradiance in W/m$^3$, $\lambda$ is the radiation wavelength in m (or nm as commonly used), $T$ is the blackbody's temperature in K, where the temperature of the sun = 5777 K, $h$ is Planck's constant = $6.62606896 \times 10^{-34}$ J s, $c$ is the speed of light in vacuum = $2.99792458 \times 10^8$ m/s, $k_B$ is Boltzmann constant = $1.3806503 \times 10^{-23}$ J/K [6].

The wavelength $\lambda$ is connected to the speed of light $c$ and the radiation frequency $v$, expressed in 1/s, as follows

$$\lambda = \frac{c}{v} \tag{2.2}$$

Because of the large distance between the earth and the sun, and the relatively high surface area of the sun compared to earth causing a decrease in the light intensity leaving the sun and reaching the earth, Eq.(2.1) should be multiplied by a

geometrical factor in order to obtain the effective solar spectral irradiance [6]. This factor is the ratio $A_s/A_{Au}$, where $A_s$ is the surface area of the sun, and $A_{Au}$ is the surface area of a sphere that having a radius equal to the earth's mean orbit, and so

$$E_{E\lambda}(\lambda, T) = E_{e\lambda}(\lambda, T)\frac{A_s}{A_{Au}} \tag{2.3}$$

In addition to Eq.(2.3), actual data of the wavelength and the corresponding spectral irradiance are available at the U.S. National Renewable Energy Laboratory (NREL) website [7] for AM0, at the top of the earth's atmosphere, and AM1.5, at the earth's surface. Figure 2.1 shows the solar spectral irradiance $E_{E\lambda}$ as a function of the wavelength $\lambda$ for AM0 and AM1.5, data are taken from NREL website [7].

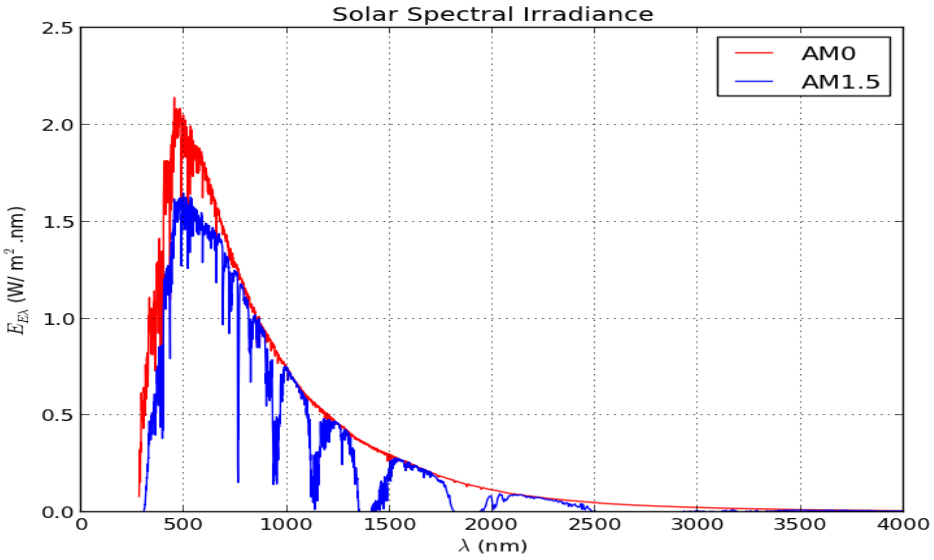


Figure 2.1: Solar Spectral irradiance for AM0 and AM1.5

To find the total irradiance $E_s$, which is the total power per unit area $W/m^2$, one can integrate the spectral irradiance with respect to the wavelength between two limit values. In addition, the energy of a photon can be expressed as

$$E_{ph} = \frac{hc}{\lambda} \tag{2.4}$$

## 2.3 Photoelectrochemical Cell

The main concept of a PEC cell is to use solar radiation to provide the energy required to drive a sequence of redox reactions needed for the electrolysis of water to produce hydrogen as the main product, and oxygen as a side product. The PEC cell consists of three main parts: the anode, the cathode and the electrolyte. The anode is the electrode at which oxidation reactions occur; on the other hand, the cathode is the counter electrode at which reduction reactions occur. The electrolyte is the media where ions can transfer from one electrode to the other, and it can either be solid or liquid. Figure 2.2, which is recreated based on Figure 2 in T. Bak et al. [2], shows a PEC cell diagram with the redox reactions occurring at the photoanode and cathode.

## 2.4 $TiO_2$ 'Optical' Properties

Titanium dioxide $TiO_2$ is an n-type semiconductor, even when not doped with electron donors atoms, due to oxygen deficiency resulting in oxygen vacancies and titanium interstitials in the $TiO_2$ lattice [8].

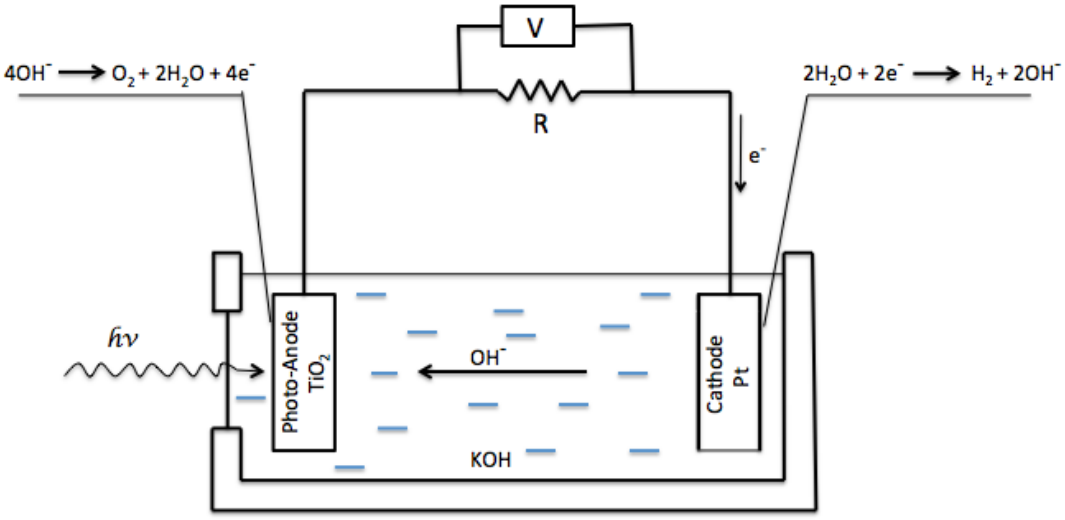


Figure 2.2: A PEC diagram with redox reactions at electrodes [2]

$TiO_2$ has a wide bandgap of about 3 eV [5]; thus, it can absorb photons with energies greater than 3 eV. In other words, according to Eq.(2.4) the critical wavelength of $TiO_2$ is $\lambda_{bg} = hc/3 = 413$ nm; therefore, only photons with wavelengths less than 413 nm can be absorbed by $TiO_2$. This wide bandgap is a disadvantage since it allows only a small portion of the solar spectral irradiance to be absorbed. Figure 2.3 shows the small fraction that can be absorbed by $TiO_2$ indicated by the area under the curve left to the black vertical line at $\lambda = 413$ nm.

Another important material property in the PEC cell model is the absorption coefficient. It describes how long the light can pass through a material without being absorbed [9]. It is a material property that is usually found experimentally and it has a unit of 1/length (usually in 1/cm). The absorption coefficient $\alpha$ of $TiO_2$ is a function of wavelength.

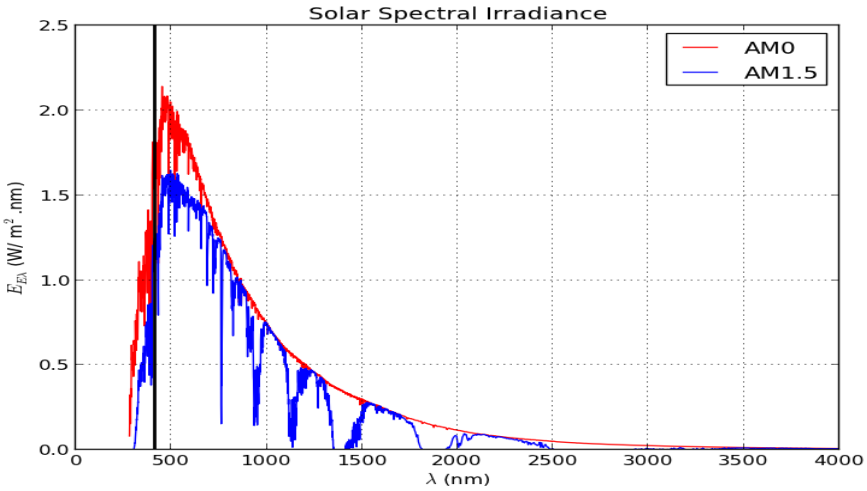


Figure 2.3: The fraction of the solar spectral irradiance absorbed by $TiO_2$

## 2.5 Photoanode

Following the Gratzel cell, also known as the dye-sensitized solar cell, $TiO_2$ must be in contact with the electrolyte since the surface reactions occur at the $TiO_2$/electrolyte interface. Therefore, the solar radiation has to travel through $SiO_2$ and ITO before it reaches $TiO_2$. In addition, when modeling or depositing $TiO_2$ on substrates for photovoltaic applications, a very important crucial issue to address is to make sure that the transparent conducting oxide layer on top of the quartz has a band gap greater than $TiO_2$. Since $TiO_2$ has a band gap of 3 eV, it can only absorb photons with energy greater than 3 eV, or in other words, with photons at wavelengths less than or equal 413 nm. Thus, if $TiO_2$ were deposited on a glass substrate with a TCO of band gap less than or equal to 3 eV, then the TCO would absorb the photons with wavelengths from zero to 413, and only the photons

with wavelengths greater than 413 will pass through the TCO; however, $TiO_2$ is transparent to these photons at that wavelength and no absorption will occur. In addition, as the difference between the TCO and the $TiO_2$ band gaps increase, with TCO band gap being the greater, more photon absorption will occur in $TiO_2$ film leading to better performance.

Quartz (SiO2) has a band gap of about 9 eV [10], while ITO has a band gap of 3.75 eV [11], [12]. Both band gaps are large enough to allow a sufficient amount of photons to pass to $TiO_2$ deposited film. Figures 2.4 and 2.5 show the solar spectral irradiance with the fraction of light that can be absorbed by ITO (shown by the green line) and $TiO_2$ (shown by the black line).

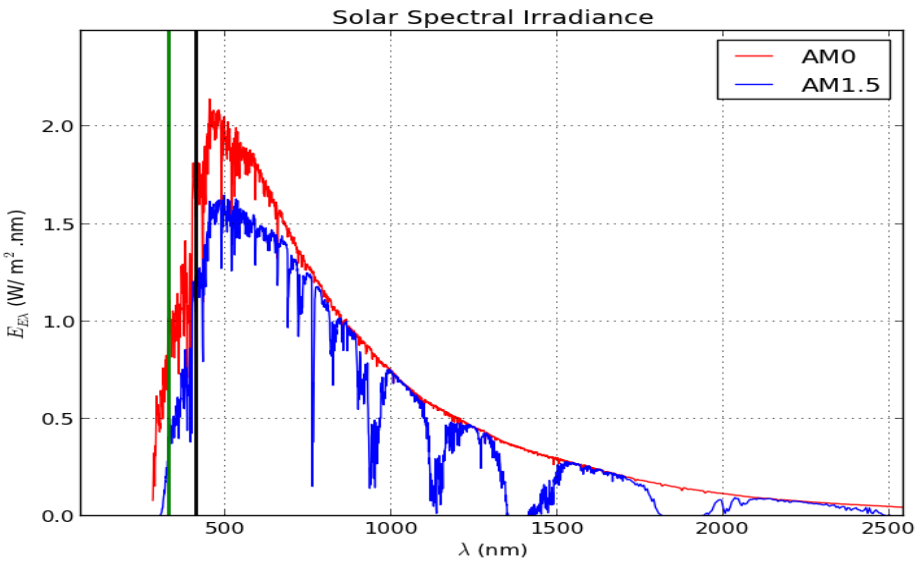


Figure 2.4: The fraction of the solar spectral irradiance that can be absorbed by ITO (green line) and $TiO_2$ (black line)

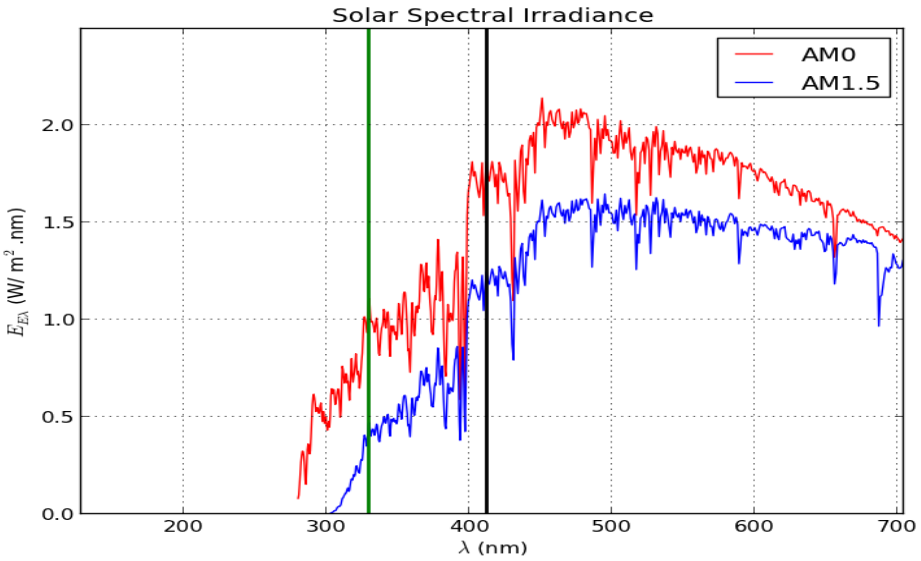


Figure 2.5: A closer look of figure 2.5

## 2.6 Electron/Hole Pair Generation Rate

When a photon is absorbed by $TiO_2$, an electron is promoted from the valence band to the conduction band, leaving a hole in the former. This electron/hole generation rate depends on the properties of the material itself, such as the bandgap and the absorption coefficient, thickness of the material, and it also depends on the light intensity falling on it. The Beer-Lambert law states that the light intensity falling on a slab surface decreases exponentially as it penetrates through the slab as follows

$$I_t(x) = I_o(0)e^{-\alpha x} \tag{2.5}$$

where $I_t$ and $I_o$ are the light intensity at slab depth x and at the surface (x=0) respectively. This law enables us to capture the electron/hole pair generation rate [9]:

$$g(\lambda, x) = [1 - R(\lambda)]\, \alpha(\lambda)\, N_0(\lambda)\, e^{-\alpha x} \tag{2.6}$$

where g is the spectral photo-generation rate per unit volume; i.e., (e/h pair)/ ($m^3$ nm s), R is the reflectivity of the surface expressed as a fraction, $N_0$ is the spectral photon flux density in photons/($m^2$ nm s) [9]. Given the wavelength dependence of the AM1.5 spectral (Figure 2.1) and Planck's Law (Eq.2.1), the charge carriers generation rate is different for each wavelength. To find the total generation rate, Eq.(2.6) is integrated with respect to the wavelength between limits where the absorption of photons occur (i.e., for wavelength less than or equal to the bandgap wavelength)

$$G(x) = \int_{\lambda_o}^{\lambda_{bg}} g(\lambda, x) \mathrm{d}\lambda \tag{2.7}$$

where G is the total generation rate per unit volume. In addition, for a slab of thickness $l$, the total generation rate per unit area across the entire thickness is

$$G_t = \int_0^l G(x) \mathrm{d}x \tag{2.8}$$

## 2.7 Redox Reactions at Photo-Anode and Cathode

For the electrolysis of water, the reaction mechanism is different for acidic and basic electrolytes. For a basic electrolyte of 1 molar KOH (pH=14), the surface reaction mechanisms [6] is listed below. At the anode where oxidation occurs, the surface reactions are as follows:

$$\mathrm{OH^- + S} \longrightarrow \mathrm{\underset{|}{\overset{}{OH}} + e^-} \quad (\mathrm{S})$$

$$\mathrm{\underset{|}{\overset{}{OH}} + OH^-} \longrightarrow \mathrm{\underset{|}{\overset{}{O}} + H_2O + e^-} \quad (\mathrm{S})$$

$$\mathrm{\underset{|}{\overset{}{O}} + \underset{|}{\overset{}{O}}} \longrightarrow \mathrm{2\,S + O_2} \quad (\mathrm{S}\ \mathrm{S})$$

The net half reaction is

$$\mathrm{4OH^-(aq)} \longrightarrow \mathrm{O_2(g) + 2\,H_2O(l) + 4\,e^-} \qquad \mathrm{E^o = -0.40V}$$

At the cathode where reduction occurs, the surface reactions are:

$$\mathrm{H_2O + S} \longrightarrow \mathrm{\underset{|}{\overset{}{H}} + OH^-} \quad (\mathrm{S})$$

$$\mathrm{\underset{|}{\overset{}{H}} + e^-} \longrightarrow \mathrm{\underset{|}{\overset{}{H}}} \quad (\mathrm{S})$$

$$\mathrm{\underset{|}{\overset{}{H}} + \underset{|}{\overset{}{H}}} \longrightarrow \mathrm{2\,S + H_2} \quad (\mathrm{S}\ \mathrm{S})$$

The net half reaction is

$$\mathrm{2H_2O(l) + 2\,e^-} \longrightarrow \mathrm{H_2(g) + 2\,OH{-}(aq)} \qquad \mathrm{E^o = -0.83V}$$

The net cell reaction is

$$2H_2O(l) \quad \longrightarrow \quad 2\,H_2(g) + 2\,O_2(g) \qquad\qquad E^{o}_{cell} = -1.23V$$

where S represent an adsorption site, $\underset{|}{\overset{OH}{S}}$, $\underset{|}{\overset{O}{S}}$, and $\underset{|}{\overset{H}{S}}$ are the adsorbed hydroxyle, oxygen, and hydrogen, respectively.

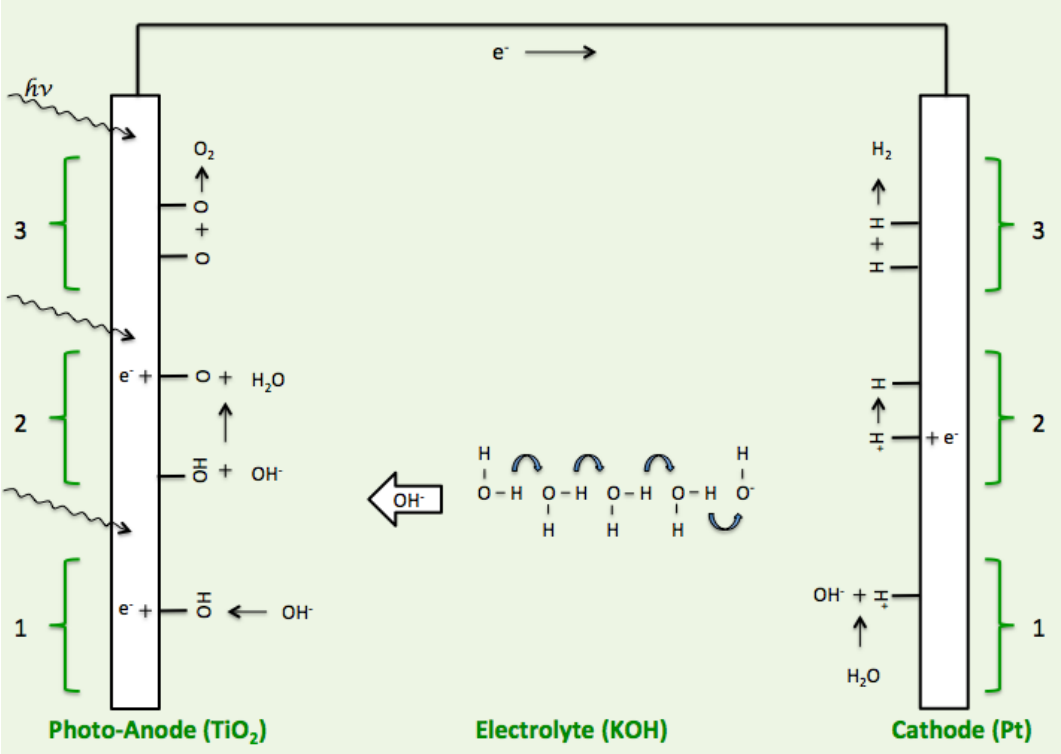


Figure 2.6: Schematic diagram of the cell showing the surface reactions and the charge-jumping mechanism.

As the electron hole pair is generated, the charge carriers are separated due to the junction formed between $TiO_2$ and the electrolyte (more details will be provided in the next section). The electrons move through the external circuit to the cathode (Pt), while the holes will oxidize the hydroxyl ions ($OH^-$) to produce oxygen gas

($O_2$) and water liquid ($H_2O$). Meanwhile, the electrons reaching the cathode will reduce the water to produce hydrogen gas ($H_2$) and hydroxyl ions ($OH^-$) which will move through the electrolyte to the anode surface to be oxidized. The movement of the $OH^-$ ions through the electrolyte to the anode follows the charge-jumping mechanism given by the proton transfer sequence [6]. Figure 2.6 illustrates the charge jumping mechanism as well as the surface reactions, where the numbers 1,2, and 3 on the figure correspond to the first, second, and third steps of the oxidation and reduction reaction.

## 2.8 Band Model Representation

In a semiconductor, the Fermi level is the maximum occupied energy level that electrons can occupy at a temperature of zero Kelvin. For an intrinsic semiconductor, the Fermi level lies approximately half way between the valence and conduction band. For a p-type semiconductor, where holes are the dominant charge carriers, the Fermi level is near the valence band. On the other hand, for an n-type semiconductor, where electrons are the dominant charge carriers, the Fermi level is near the conduction band. Figure 2.7 illustrates the initial conditions of the cell components without contact and without light, where $\Phi_m$ is the Pt work function, which is the minimum energy required to ionize an electron and move it to the vacuum level outside the metal [9].

When $TiO_2$ is submerged in the liquid electrolyte, the Fermi level of $TiO_2$ is higher than the redox potential of the electrolyte; thus, electrons will transfer from the semiconductor to the electrolyte causing an upward band bending [13]. In addition, a space charged region (or a depletion layer) is formed between $TiO_2$ and the electrolyte, with positive charges associated with the semiconductor side, and negative charges at the electrolyte side [13]. This junction plays a key role in the charge separation of the electron hole pair generated from the absorbed photons.

For a closed circuit (i.e., with Pt electrode connected as cathode), the Fermi level of the Pt will also equalize with the Fermi level of $TiO_2$ and the redox potential of the electrolyte as in Figure 2.8. For the redox reactions to occur at the anode and cathode, the Fermi level of the anode should be higher than the $O_2/H_2O$ potential, which is the case at most times; however, the Fermi level of the cathode should also be greater than the $H^+/H_2$ potential [2]. Therefore, at some cases, even when light is induced (Figure 2.9), charge carriers will be generated in the semiconductor but no reactions will occur requiring an external bias to shift the cathode Fermi level above the $H^+/H_2$ potential and start the reactions [2] as in Figure 2.10. Figures 2.7-2.10 are recreated based on T. Bak et al. Figures 4-7 [2].

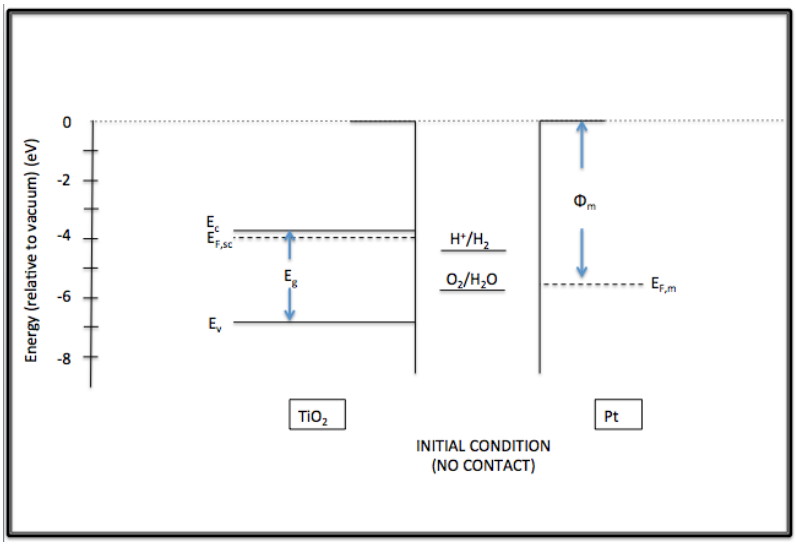


Figure 2.7: Initial cell conditions without contact [2]

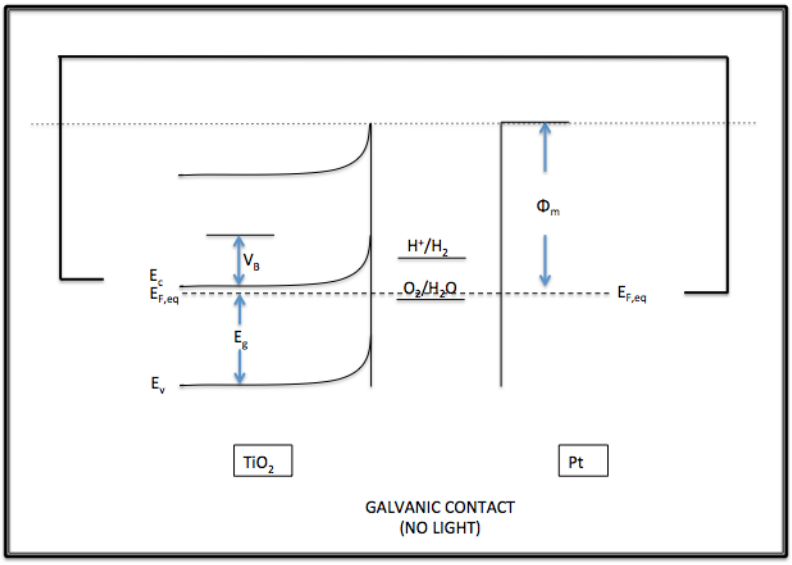


Figure 2.8: Cell condition with contact but no light is induced [2]

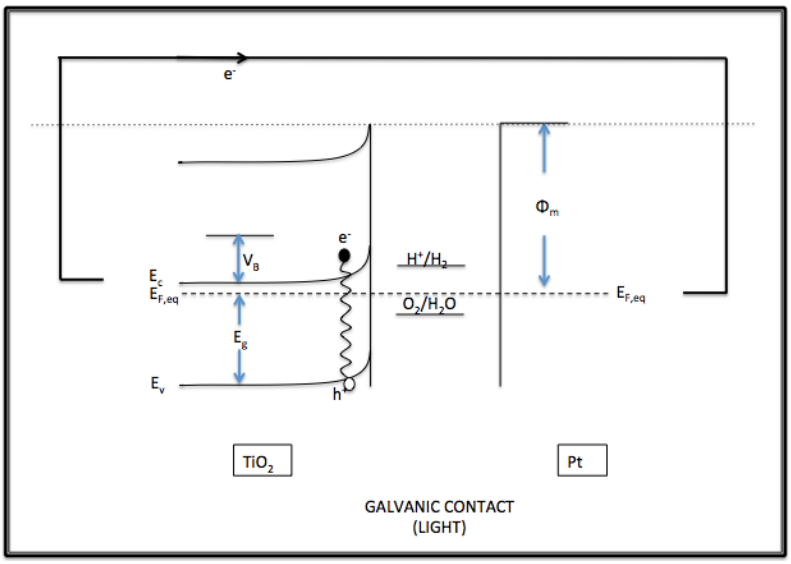


Figure 2.9: Cell contact with light illumination [2]

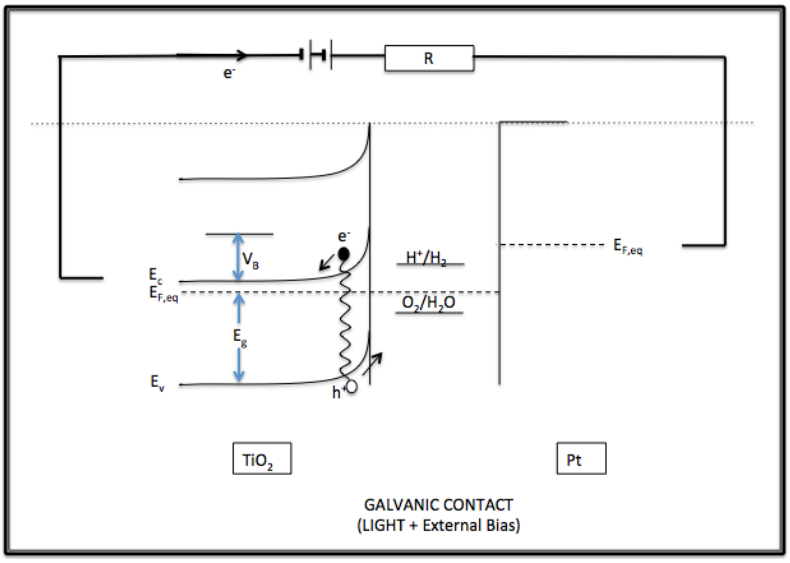


Figure 2.10: Light illumination with external bias [2]

## 2.9 Literature Review

The production of hydrogen gas from the process of water electrolysis is not new to the field; in fact, it was discovered about 200 years ago [1]. As early as 1800, William Nicholson and Anthony Carlisle discovered electrolysis and applied voltaic current to decompose water into gases, which were later recognized as hydrogen and oxygen gases [1], [5]. They also noticed that increasing the current used would increase the amount of gases produced [5]. After this discovery, the science of electrochemistry has been and is being developed even today.

In 1972, Fujishima and Honda [14] were the first to utilize and report a photoelectrochemical cell with $TiO_2$ as a photoanode and Pt as a cathode, with an electrolyte of pH = 4.7. They found that current started to flow at light wavelengths of less than 413 nm (corresponding to $TiO_2$ band gap of 3.0 eV). Additional bias voltage was applied (0.25-0.5 V) to enable the process [14], [1]. Using 500 W Xe lamp, they were able to measure the current of a few mA. In 1975, Fujishima, Honda and Kohayakawa used a $TiO_2$ oxidation layer on Ti metal instead of a single crystal $TiO_2$ as they did in 1972 [15], [2]. They tested three different methods to form the oxide film electrodes; electrochemical formation of the oxide film on Ti metal, thermal formation of the oxide film using an electric furnace, and thermal formation of the oxide using a gas burner. The first two methods resulted in a photocurrent of about one-tenth of the photocurrent obtained using a single crystal, but the last method, which had an oxide film thickness greater than the other two methods, resulted in a photocurrent similar to the single crystal case [15]. As discussed in their

paper, the performance difference in the three different oxide films is primary due to the difference in the electric resistance, and oxide film thickness [15]. This point is important since, in this research, $TiO_2$ film thickness is one of the optimization variables used to optimize the production of hydrogen moles.

Enormous amounts of experiments and publications have been reported from that time until now. Some people used sunlight, but accomplished very little overall efficiency (solar conversion efficiency). Others used special lamps to get more light intensity. Encouraged by the work of Fujishima and Honda, researchers have been looking for new oxide materials candidates as PEC cells photoanodes, such as $SrTiO_3$ and $KTaO_3$, to eliminate the use of external bias; however, the proposed candidates light conversion efficiencies were found to be less than that of $TiO_2$, not forgetting the $TiO_2$ advantage of corrosion resistance [16].

Since $TiO_2$ absorbs photons with energy up to or greater than 3 eV, in 1976, Morisaki et al. [17] proposed the use of a hybrid $TiO_2$-Si solar cell electrode, where the silicon cell would help to utilize the solar spectral absorption between 1.2 and 3 eV. Their cell mainly consists of the hybrid electrode as photoanode with a $TiO_2$ film thickness of 500 nm, a Pt as cathode, and a 0.1 M NaOH electrolyte. Figure 2.11, which is recreated based on Figure 18 in [2], shows a schematic diagram of the hybrid cell used. Although the reported conversion efficiency was relatively small (only 0.1 % with sunlight illumination), their research contributed in the field since they introduced a good idea in which the spectral irradiance is better utilized, and an internal anodic bias is created by the electromotive force of the solar cell [17].

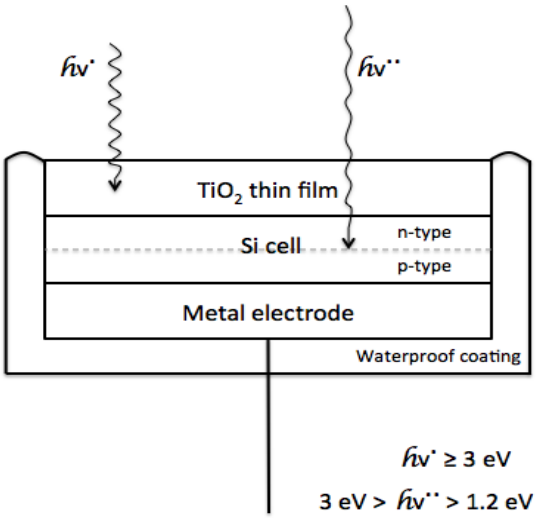


Figure 2.11: Schematic diagram of the hybrid photoanode [2]

In 1977, Ghosh and Maruska used a cell consisting of $TiO_2$ as an anode, Pt as a cathode, and a basic electrolyte of 5 M KOH under sunlight illumination [18]. The reported efficiencies were 0.6% for Al-doped $TiO_2$ with a 0.4 V bias voltage. Although the published experiments are informative, we cannot determine how hydrogen production rate and the photocurrent change with $TiO_2$ and ITO thickness since each one has different cell conditions, such as film deposition method, temperature, electrolyte type and pH, doping level (if any) and light source used. Thus, a useful model relating the hydrogen production with electrode film thickness is needed, in which one can find the optimal film thickness that yields to the optimal hydrogen production rate.

The optimization of a PEC cell with $TiO_2$ as a photoanode is not new to the field; however, little work is done with $TiO_2$ thickness as the optimization variable. A study done by Mishra et al. [19] investigated the effect of oxidation temperature and

oxygen flow rate on the photocurrent and hydrogen production. Their cell basically consists of $TiO_2$ electrode (at different oxidation temperatures), with Pt counter electrode and a 1 M NaOH electrolyte. They found that the optimal photocurrent was 0.93 $mA/cm^2$ corresponding to an oxidation temperature of 750 °C with oxygen flow rate of 350 ml/min [19].

An interesting paper published in 2007 [20] centered around the preparation of $TiO_2$/ITO photoelectrodes via the sol-gel method where the research investigated several aspects including the effect of the electrode film thickness on the generated photocurrent. They prepared several electrodes with thicknesses of 0.15, 0.19, 0.27, and 0.34 $\mu$m, and they concluded that as the thickness increased (from 0.15 up to 0.27 $\mu$m) the photocurrent was slightly decreased due to the increased electrical resistance of $TiO_2$ film that outweighed the increase in the electron/hole pair generated. As the film thickness increased above 0.27 $\mu$m, the decrease in the photo current had a larger slope, since no huge increase in the number of electron hole pair was generated to compensate the increase in the $TiO_2$ electrical resistance.

With the increasing interest in renewable energy applications, different materials were and are still being tested as a photoanode.

# Chapter 3: Methodology

As explained in Chapter 2, to compute the total electron/hole pair generation rate $G_t$ at a $TiO_2$ thickness of $x_2$, one should calculate the spectral photo-generation rate per unit volume ($g$) as given in Eq.(2.6).

$$g(\lambda, x_1, x_2) = [1 - R(\lambda, x_1)]\, \alpha(\lambda)\, N_0(\lambda)\, e^{-\alpha x_2}$$

$N_0$ is the spectral photon flux density in photons/($m^2$ nm s), and it is calculated by dividing the spectral irradiance at each wavelength by the photon energy

$$N_0(\lambda) = \frac{E(\lambda)}{E_{ph}} = \frac{E(\lambda)\lambda}{hc} \tag{3.1}$$

$g$ is mainly a function of $\lambda$ and $x_2$; however, since the reflection between the surfaces depends on ITO thickness $x_1$, then $g$ is considered a weak function of $x_1$.

## 3.1 Light Reflection $R$

To estimate the reflection of normal incident radiation between the surfaces of $SiO_2$, ITO, and $TiO_2$, the following equation is used [6]:

$$R(\lambda, x_2) = \frac{\hat{r}_{01}^2 + \hat{r}_{12}^2 + 2\hat{r}_{01}\hat{r}_{12}cos\phi_d}{1 + \hat{r}_{01}^2\hat{r}_{12}^2 + 2\hat{r}_{01}\hat{r}_{12}cos\phi_d} \tag{3.2}$$

The first and second surfaces reflected wave phase difference is given by [6]:

$$\phi_d = \frac{2\pi}{\lambda} n_1(2x_1) \tag{3.3}$$

The single interface reflectances $\hat{r}_{01}$ and $\hat{r}_{12}$, shown in Figure 3.1, can be defined as:

$$\hat{r}_{01} = \frac{n_1 - n_0}{n_1 + n_0} \tag{3.4}$$

$$\hat{r}_{12} = \frac{n_2 - n_1}{n_2 + n_1} \tag{3.5}$$

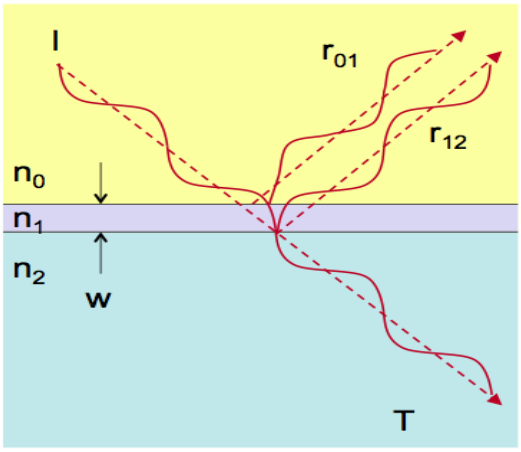


Figure 3.1: Thin film reflectances [6]

where $n_0 = 1.46$ [21], $n_1 = 2.20$ [21], $n_2 = 2.87$ [21] are the refractive indices of $SiO_2$, ITO and $TiO_2$ respectively. Equations (3.4) and (3.5) suggest that as the difference between the refractive indices of two materials decrease, the light reflection between these two materials is reduced. The effect of the KOH solution electrolyte is not considered for simplicity, since the refractive index of KOH solution is about 1.42 [22], which is close to $n_0$ and, thus, no major reflection occurs.

## 3.2 Absorption Coefficient $\alpha$

The absorption coefficient $\alpha$ is a function of wavelength, and is usually found experimentally. A study published by Kil Lee [23] showed the effect of substrate temperature on some of the optical properties, including the absorption coefficient, of $TiO_2$ thin films deposited on ITO coated glass substrates. The absorption coefficient data as a function of photon energy were extracted from Figure 5 in Kil Lee [23], and using Eq.(2.4), the absorption coefficient was plotted as a function of the photon wavelength as shown in Figure 3.2. As a simplified curve fitting, the extracted data were divided into three regions as shown in Figure 3.2.

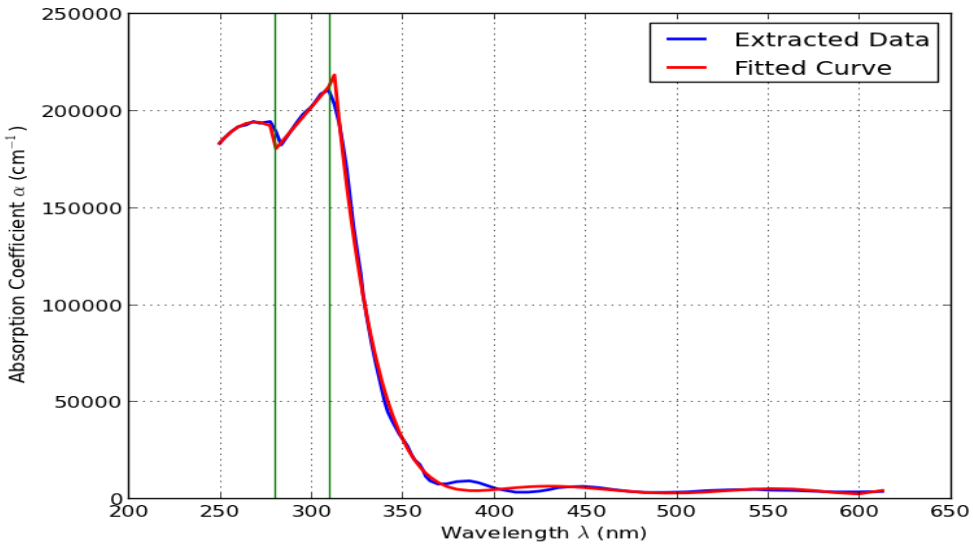


Figure 3.2: Absorption coefficient as a function of photon wavelength

$$\alpha(\lambda) = \begin{cases} -(a_1)\lambda^2 + (a_2)\lambda - (a_3) & : 249 \leq \lambda \leq 280 \\ (b_1)\lambda - (b_2) & : 280 < \lambda \leq 310 \\ (c_1)\lambda^6 - (c_2)\lambda^5 + (c_3)\lambda^4 - (c_4)\lambda^3 + (c_5)\lambda^2 - (c_6)\lambda + (c_7) & : 310 < \lambda \leq 612 \end{cases} \tag{3.6}$$

The values of the fitted curve coefficients are given in Table 3.1.

Table 3.1: Absorption coefficient fitted curve coefficient

| $a_1$ | $a_2$ | $a_3$ | $b_1$ |
|---|---|---|---|
| 28.7 | 15.43 $\times 10^3$ | 18.81 $\times 10^5$ | 11.04 $\times 10^2$ |
| $b_2$ | $c_1$ | $c_2$ | $c_3$ |
| 12.85 $\times 10^4$ | 1.38 $\times 10^{-8}$ | 4.08 $\times 10^{-5}$ | 5 $\times 10^{-2}$ |
| $c_4$ | $c_5$ | $c_6$ | $c_7$ |
| 32.5 | 11.81 $\times 10^3$ | 22.73 $\times 10^5$ | 18.11 $\times 10^7$ |

An important issue to consider when using the absorption coefficient fitted curve equation in the model calculations is using large significant figures to have the precision required, since the values of the absorption coefficient are too large and sensitive for any minor difference in the fitted equation coefficients. At first, a piece-wise linear approximation was used to fit the data; however, some of the fitted absorption coefficient data were negative causing wrong and misleading charge

carriers generation results; for that reason, a more sophisticated curve fitting was used as in Eq.(3.6). Furthermore, the unusual behavior of the absorption coefficient curve in Figure 3.2, especially the two peaks for small wavelength values, might be due to the experimental settings used. For instance, the $TiO_2$ used in Kil Lee [23] has a band gap greater than 3 eV, which can account for the early decrease in the absorption data before the critical wavelength of 413 nm, which corresponds to 3 eV. However, in this thesis, the absorption coefficient data of wavelengths less than 330 is not used, and only the absorption coefficient data with wavelengths between 330 nm and 413 nm are used since $TiO_2$ will absorb the light of wavelengths in this range only.

## 3.3 Total Generation Rate and Recombination Rate

To calculate the generation rate at a specific film depth, the electron/hole pair generation rate at each individual wavelength is to be added. Thus, one can integrate the spectral generation rate $g$ with respect to the wavelength, keeping in mind that the integration limits are defined by the wavelength range at which electron hole generation is possible [9]. Therefore, the integration limits would be from $\lambda = 330$nm, which is the critical wavelength of ITO, to $\lambda = 413$nm, which is the critical wavelength of $TiO_2$.

$$G(x_1, x_2) = \int_{330}^{413} g(\lambda, x_1, x_2)\mathrm{d}\lambda \tag{3.7}$$

where $x_1$ and $x_2$ are ITO and $TiO_2$ film thicknesses, respectively (in nm). $G(x)$ has units of (e/h pair)/$m^3$ or (e/h pair)/$m^2$nm if the thickness is taken in nm. It provides us with the electron/hole pair generation rate of a certain area of substrate at a certain $TiO_2$ film depth $x_2$. The total generation rate per unit area at a $TiO_2$ film of thickness $l$ is found by:

$$G_t(x_1, l) = \int_0^l G(x_1, x_2)\mathrm{d}x_2 \tag{3.8}$$

One of the nonidealities that may affect the performance of the PEC cell is the electron hole recombination rate. Among the different types of the bulk recombination, the spontaneous emission (also known as the radiative recombination) is the the most important one in photovoltaics [9]. The recombination rate is given by [9]:

$$r_{sp}(E) = \frac{2\pi n_2^2}{h^3c^2}\frac{\alpha(E)E^2}{\exp[(E-\Delta\mu)/k_BT]-1} \tag{3.9}$$

where $r_{sp}$ is the volumetric e/h recombination rate per photon energy (e/h recombined)/ ($m^3$eV). $\Delta\mu$ is the chemical potential of radiation (or the quasi-Fermi level separation) which is equal to the difference between electron quasi-Fermi level ($E_{Fn}$) and hole quasi-Fermi level ($E_{Fp}$) [9]. Another helpful definition of $\Delta\mu$ is given by [24]:

$$\Delta\mu = hv(1-\frac{T}{T_{sun}}) = E(1-\frac{T}{T_{sun}}) \tag{3.10}$$

The total recombination rate is found by integrating Eq.(3.9) with respect to photons energy [9]:

$$U = \int_0^\infty r_{sp}(E)\mathrm{d}E \tag{3.11}$$

In addition, to obtain the net recombination rate, one must subtract the recombination rate at $\Delta\mu = 0$ which represents the thermal equilibrium state, as in Eq.(3.12).

$$U^{net} = \int_0^\infty r_{sp}(E)\mathrm{d}E - \int_0^\infty r_{sp}(E)|_{\Delta\mu=0}\mathrm{d}E \tag{3.12}$$

$U^{net}$ has units of (number of e/h recombined)/$\mathrm{m}^3$; thus, to get the recombination rate at certain $TiO_2$ film thickness $l$, $U^{net}$ is multiplied by $l$

$$U^{total} = U^{net} \times l \tag{3.13}$$

The net electron/hole pair available to derive the process is

$$G_{net}(x_1, x_2) = G_t(x_1, x_2) - U^{total} \tag{3.14}$$

## 3.4 External Current Model

The governing equation used to describe the system is as follows [6], [9]:

$$I = -I_{ph} + I_o \left[\exp\left(q\frac{V - IR_s}{\beta k_B T}\right) - 1\right] \tag{3.15}$$

where $I$ is the current passing through the external circuit (A), $I_{ph}$ is the photocurrent generated from radiation (A), $I_o$ is the dark current, which is the current (A) generated in the dark as a result of potential difference when a load is connected. V is the voltage (V), $R_s$ is the series resistance ($\Omega$), and $\beta$ is the diode non-ideality factor, typically ranging from 1–2, and is assumed to be 1 for the model.

The photocurrent is calculated from the net electron/hole pair generated and the unit charge q:

$$I_{ph}(x_1, x_2) = qG_{net}(x_1, x_2) \tag{3.16}$$

To find the dark current, open circuit conditions can be used, i.e., when the external current is zero. Therefore, from Eq.(3.16) the dark current can be calculated as:

$$I_o(x_1, x_2) = \frac{I_{ph}(x_1, x_2)}{\exp\left(q\frac{V_{oc}}{\beta k_B T}\right) - 1} \tag{3.17}$$

where $V_{oc}$ is the open circuit voltage (V), which can be estimated as a function of band gap [6], [25]:

$$V_{oc} = E_{bg}\left(1 - \frac{T}{T_{sun}}\right) - \frac{k_B T}{q}\ln\frac{4n_2^2}{X} \tag{3.18}$$

where X is the sunlight concentration factor, taken as 1 for a regular sunny day.

## 3.5 Series Resistance

Some of the nonidealities added to the model are the series resistance of the cell components, such as $TiO_2$ electrical resistance, ITO sheet resistance, Pt electrode resistance and the electrolyte (KOH) resistance. These resistances are added together as a series resistor in Eq.(3.15)

The sheet resistance of ITO is a function of film thickness $x_1$. As the thickness increases, the sheet resistance decreases. ITO sheet resistance data were obtained from Sigma-Aldrich website [26] – [29], and fitted exponentially as shown in Figure 3.3.

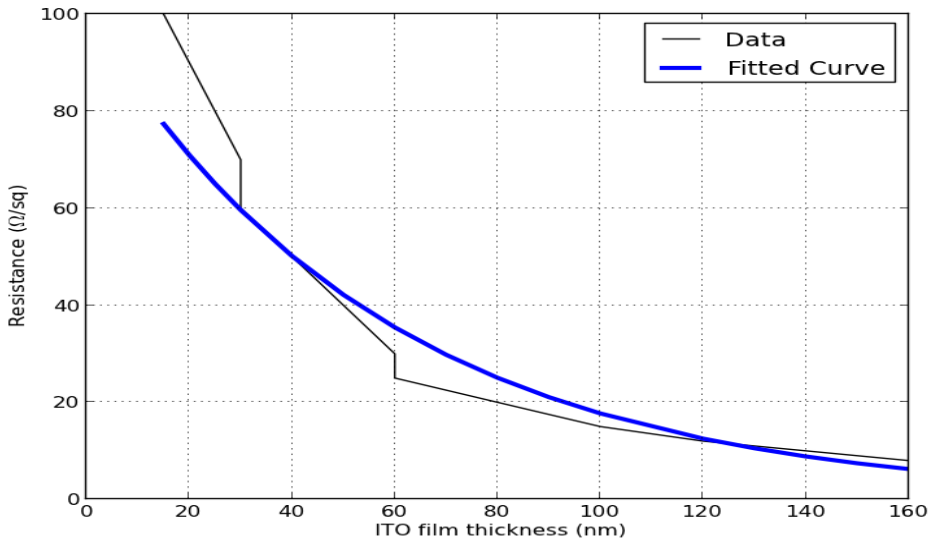


Figure 3.3: Sheet resistance of ITO film as a function of ITO thickness $x_1$

In addition, $TiO_2$ electrical resistance can be calculated from the relation:

$$R = \rho \frac{L}{A} \tag{3.19}$$

where $\rho$ is the resistivity ($\Omega.cm$), L is the length direction at which the current is conducted. For this case, L is the thickness of $TiO_2$ film. A is the cross-sectional area at which the current is conducted, and it is assumed to be 1 $m^2$ for our PEC model. The resistivity of TiO2 film can be estimated as $8 \times 10^4$ $\Omega$.cm [30].

The Pt electrode resistivity is $10.6 \times 10^{-8} \Omega$.m [31]. Therefore its resistance can be calculated using Eq.(3.19), where L represents the direction at which current flows (1 m), and A is the thickness (assumed to be 1 mm thick) multiplied by the electrode width (1 m), which will yield a resistance $R_{Pt}$ of $10.6 \times 10^{-5} \Omega$.

The conductivity of the KOH electrolyte is given in Figure 1 of Gilliam et al. [32]. For 1 M KOH, the conductivity is about 0.2 S/cm resulting in a resistivity

of $1/0.2 = 5$ Ω.cm. The electrolyte resistivity can also be calculated from Eq.(3.19), with L as the electrolyte path length typically of about 1 mm [33]. Hence, the electrolyte resistance is $R_{KOH} = 5 \times 10^{-5}\Omega$.

The number of hydrogen moles evolving from the cathode can be found using the assumption that each two electrons reaching the cathode will result in producing one hydrogen molecule $H_2$:

$$n_{H_2} = \frac{I}{2qA_v} \tag{3.20}$$

where $A_v$ is Avogadro's number.

Finally, the overall efficiency of the PEC cell is given by [2]:

$$\eta_c = \frac{I(1.23 - V_{bias})}{I_r A} \tag{3.21}$$

where $I$ is the external current generated at the optimum conditions, $I_r$ is the incidence of solar irradiance = 970 W/m$^2$ [2], A is the irradiated area.

# Chapter 4: Results and Discussion

## 4.1 ITO Resistance and Thickness

ITO thickness plays an important role in the rate of hydrogen generation. As mentioned in Chapter 3, ITO sheet resistance data were obtained from the Sigma-Aldrich website [26] - [29], and fitted exponentially (Figure 3.3) as follows:

$$R_{ITO} = 100.381 \times \exp(-0.0173497 \times x_1) \tag{4.1}$$

where $x_1$ is ITO film thickness in nm, and $R_{ITO}$ is in $\Omega$ . As the thickness of ITO increases, the resistivity decreases exponentially, leading to higher external current and, therefore, to a higher rate of hydrogen generation. Thus, if the thickness of ITO is to be considered as an optimization variable, the optimization problem will choose the higher value of the thickness, i.e., the upper limit of the ITO thickness constraint. As a reasonable approach, an ITO thickness $x_1 = 400$ nm will be chosen since the current is increased effectively until this thickness is reached, and no significant difference in the current is noticed above this thickness. Table 4.1 shows the current for different $TiO_2$ thickness values of 1000 nm, 3000 nm, and 7000 nm to illustrate the effective increase of the current for $x_1$ values less than 400 nm, and the small increase for values greater than 400 nm.

Table 4.1: External circuit current ($A/m^2$) at different ITO thickness $x_1$ and $TiO_2$ thickness $x_2$ values.

| $x_1$ (nm) | $x_2 = 1000$ nm | $x_2 = 3000$ nm | $x_2 = 7000$ nm |
|---|---|---|---|
| 200 | 0.882 | 0.881 | 0.880 |
| 300 | 4.98 | 4.97 | 4.94 |
| 400 | 19.5 | 26.9 | 26.3 |
| 500 | 19.8 | 28.8 | 32.6 |

Since the reflection of light R is also a function of ITO thickness $x_1$, one can expect that there might be an optimum solution of ITO film thickness $x_1$, which leads to an optimal value of external current. However, the effect of the ITO resistance on the external current is much more important than the effect of the light reflection. As a result, light reflection sinusoidal effects will appear for large values of $x_1$ after the ITO resistance effect is almost negligible. Figure 4.1 shows the sinusoidal effect of the light reflection on the external circuit current for large ITO thickness $x_1$ at a $TiO_2$ thickness of 3000 nm.

The light reflection has a small effect on the current for several reasons. Because the difference in the refractive indices of the three layers ($SiO_2$, ITO, and $TiO_2$) is not significant, the maximum value of the reflection is below 11% as shown in Figure 4.2. In addition, for a large critical wavelength material (i.e., small band

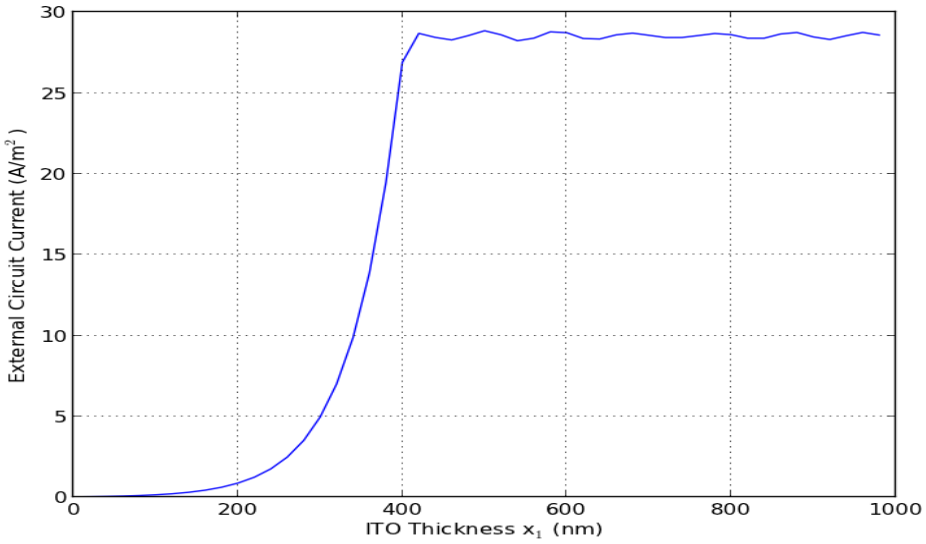


Figure 4.1: External Current at $x_2 = 3000$ nm as a function of $x_1$

gap) the effect of light reflection can be minimized by the choice of the ITO thickness, since the reflection has low frequency at higher wavelength (as in Figure 4.2).

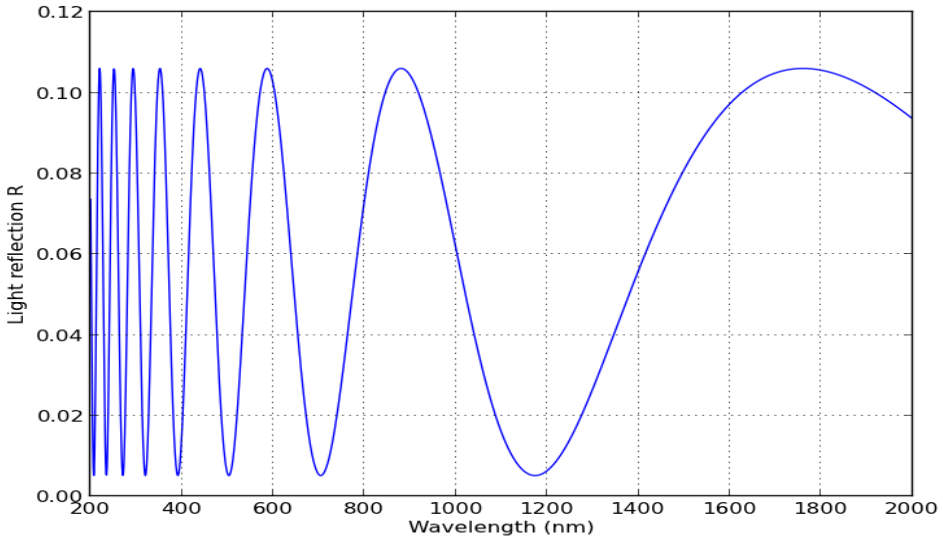


Figure 4.2: Light reflection at ITO thickness $x_1 = 400$ nm

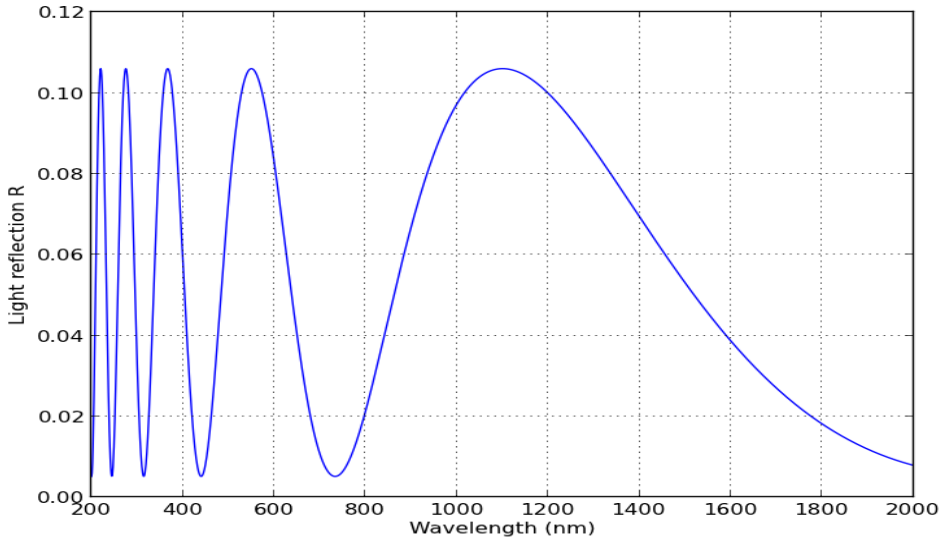


Figure 4.3: Light reflection at ITO thickness $x_1$ = 250 nm

To illustrate, if a material (other than $TiO_2$) has a critical wavelength of 1200 nm, then it is better to have an $x_1$ value = 400 nm (as shown in Figure 4.2), where the reflection is minimized at $\lambda$=1200 nm, rather than an $x_1$ value = 250 nm (as shown in Figure 4.3) where the reflection is maximized at $\lambda$=1200 nm. However, since our material $TiO_2$ has a small critical wavelength of 413 nm, the frequency of the light reflection is high, resulting in multiple minima and maxima.

## 4.2 Electron/Hole Pair Generation Rate

The electron/hole generation rate G found from Eq.(3.7) is shown in Figure 4.4 at $x_1$ = 400 nm, as a function of $TiO_2$ film depth. Figure 4.5 shows the same results but with logarithmic scale of G. The $TiO_2$ film front surface is at 0 nm, where maximum photon absorption occur leading to maximum e/h pair generation rate.

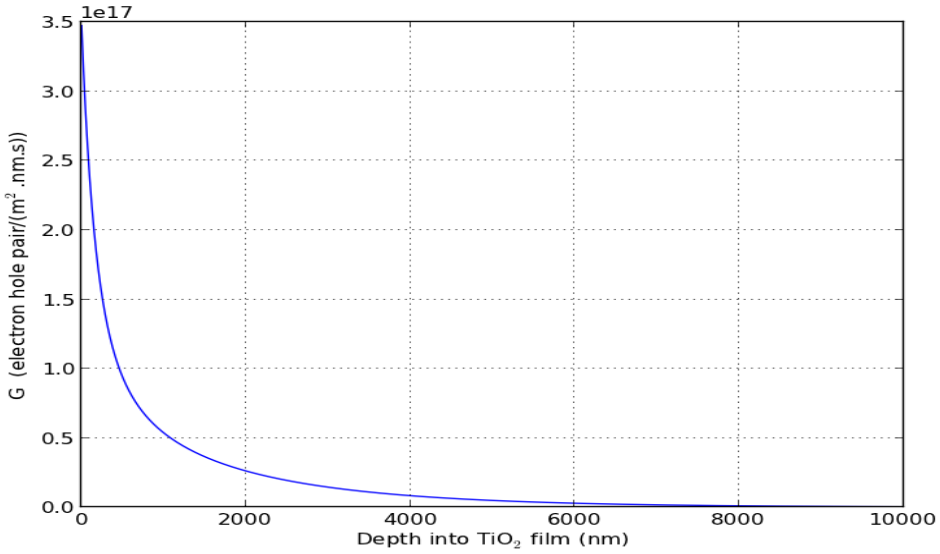


Figure 4.4: The generation rate G at $x_1 = 400$ nm, as a function of $TiO_2$ film depth

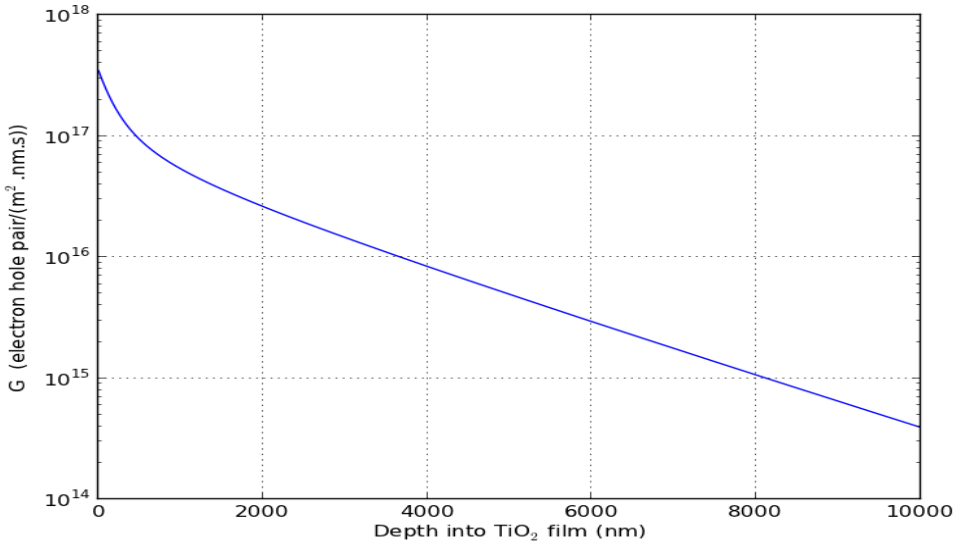


Figure 4.5: A logarithmic scale of G at $x_1 = 400$ nm, as a function of $TiO_2$ film depth

The total electron/hole pair generation rate $G_t$ found from Eq.(3.8) is plotted at $x_1 = 400$ nm, at different values of $TiO_2$ film thickness $x_2$ in Figure 4.6. The total generation rate is an increasing function, since it is the integral of the electron/hole pair generation rate G at a film depth of $x_2$, i.e., the area under the curve of Figure 4.4. Figure 4.7 shows the logarithmic result of $G_t$.

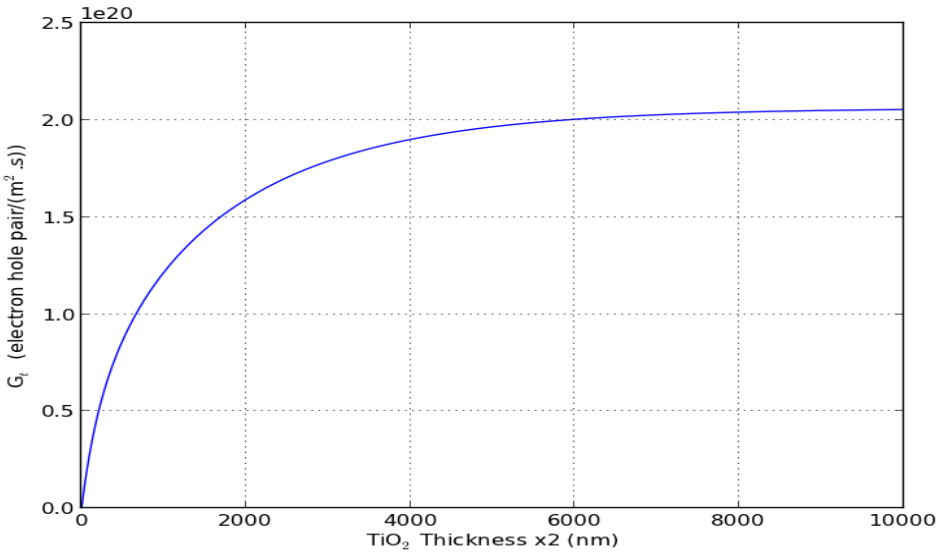


Figure 4.6: The generation rate $G_t$ at $x_1 = 400$ nm, as a function of $x_2$

## 4.3 Recombination of Charge Carriers Rate

The charge carriers bulk recombination rate is found from Eq.(3.9). Since the absorption coefficient data are fitted as a function of wavelength as in Eq.(3.6), Eq.(3.9) and (3.10) are modified to be functions of wavelength:

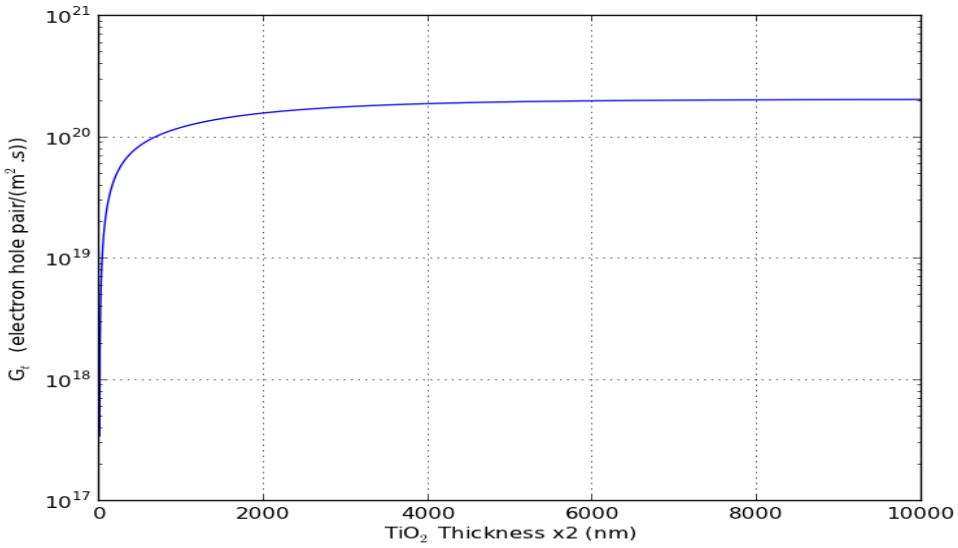


Figure 4.7: A logarithmic scale of $G_t$ at $x_1 = 400$ nm, as a function of $x_2$

$$r_{sp}(\lambda) = \frac{2\pi n_2^2}{h\lambda^2} \frac{\alpha(\lambda)}{\exp\left[\left(\frac{hc}{\lambda} - \Delta\mu(\lambda)\right)/k_B T\right] - 1} \tag{4.2}$$

$$\Delta\mu(\lambda) = \frac{hc}{\lambda}\left(1 - \frac{T}{T_{sun}}\right) \tag{4.3}$$

In addition, the total recombination rate as a function of wavelength is as follows:

$$\mathrm{d}E = -\frac{hc}{\lambda^2}\mathrm{d}\lambda \tag{4.4}$$

The lower and upper integration limits of the total recombination rate in Eq.(3.11) are zero and infinity, respectively; however, since the photon energy data range was 2 to 5 eV, these values were used as integration limits. Therefore, the total recombination rate is found to be

$$U = \int_{248}^{620} r_{sp}(\lambda)\frac{hc}{\lambda^2}\mathrm{d}\lambda \tag{4.5}$$

where $\lambda$ of 248 nm corresponds to E = 5 eV, and $\lambda$ of 620 nm corresponds to E = 2 eV, and the integration limits are reversed because of the negative sign in Eq.(4.4). Substituting in Eq.(4.5) by using our model data, the net recombination rate per unit volume following Eq.(3.12) is:

$$U^{net} = 9.197 \times 10^{12} \qquad (\text{e\h recombined})/\text{m}^3$$

$$= 9197 \qquad (\text{e\h recombined})/\text{m}^2.\text{nm}$$

Thus, the charge carriers recombination rate per unit area at $TiO_2$ thickness $x_2$ is

$$U^{total} = U^{net} \times x_2 \tag{4.6}$$

where $U^{total}$ is in (e\h recombined)/$\text{m}^2$, and $x_2$ is in nm.

## 4.4 External Circuit Current Model Parameters

The open circuit voltage is found from Eq.(3.18), taking the sunlight concentration factor X = 1, and so

$$V_{oc} = 2.75 \text{ V}$$

The open circuit voltage is high due to the high band gap of $TiO_2$. The photocurrent $I_{ph}$ is found from Eq.(3.16) at different $x_1$ and $x_2$ values, and by having $I_{ph}$ and $V_{oc}$, the dark current $I_o$ can be calculated from Eq.(3.17) at different values of $x_1$ and $x_2$, assuming the non-ideality factor $\beta = 1$, and no external bias voltage is applied ($V = 0$ V ).

$TiO_2$ electrical resistance is calculated from Eq.(3.19), with 1 $m^2$ electrode surface area

$$\begin{aligned} R_{TiO_2} &= \frac{\rho \times x_2}{A} \\ &= \frac{(8 \times 10^4 \Omega.cm)(10^7)}{10^{18}} \times x_2 \\ &= (8 \times 10^{-7}) \times x_2 \qquad \Omega \end{aligned}$$

The Pt electrode and KOH electrolyte resistances are given in Section 3.5, as follows:

$$R_{Pt} = 10.6 \times 10^{-5} \qquad \Omega$$

$$R_{KOH} = 5 \times 10^{-5} \qquad \Omega$$

The ITO resistance correlation is given in Section 4.1. Thus, the series resistance $R_s$ in Eq.(3.15) is given as the summation of these resistances:

$$R_s = R_{TiO_2} + R_{ITO} + R_{Pt} + R_{KOH}$$

Of these four resistances, the ITO resistance is the most important one, since it highly affects the current generated.

## 4.5 Optimum Value Results

Python programming language is used for calculations and simulations of the research model. The scipy.optimize package is used for the optimization problem. The optimization problem is given as

$$\begin{aligned} &\underset{x_2 \in R}{\text{minimize}} \quad I \\ &\text{s.t.} \qquad 0 \leq x_2 \leq 10,000 \qquad nm \end{aligned}$$

where the sign of the current is negative, referring to the direction of it. Thus, minimizing the negative value current will lead to having $|I|$ reaching the highest value possible.

One can notice that the external circuit current Eq.(3.15) is an implicit function owing to the existence of $I$ in the left hand side, and in the exponential of the right hand side; ergo, a numerical method is required. The Newton-Raphson method was used, and a function was created in Python, which takes $x_1$ and $x_2$ as inputs, and returns the external current value $I$.

The simulation results showed that at ITO film thickness $\mathrm{x_1}$ = 400 nm, as chosen in Section 4.1, the optimum current value $I^{opt}$ = 26.9 A for a 1 $\mathrm{m^2}$ surface area electrode, with an optimum solution of the $TiO_2$ thickness $\mathrm{x_2^{opt}}$ = 3230 nm. This value of the optimum solution $\mathrm{x_2^{opt}}$ is reasonable as we take a closer look at Figure 4.7, where the total electron/hole generation rate becomes almost constant at around 3000 - 3400 nm. Hence, after these $TiO_2$ thickness values, not many electron/hole pair are generated to overcome the effect of the increased electrical resistance of $TiO_2$ and increased charge carrier recombination rate. Figures 4.8 and 4.9 represent the external current generated as a function of $TiO_2$ thickness $x_2$ showing the optimal conditions.

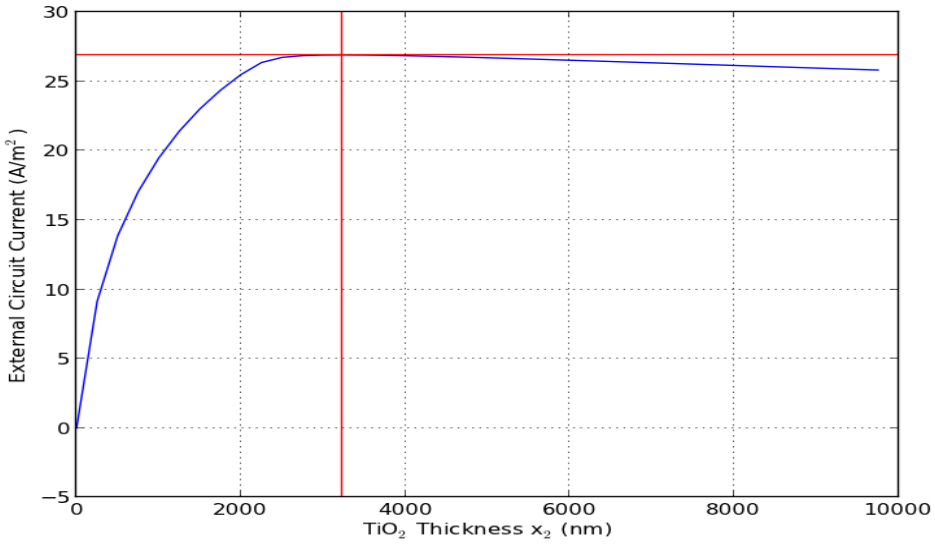


Figure 4.8: External circuit current $I$ at $x_1 = 400$ nm, as a function of $x_2$

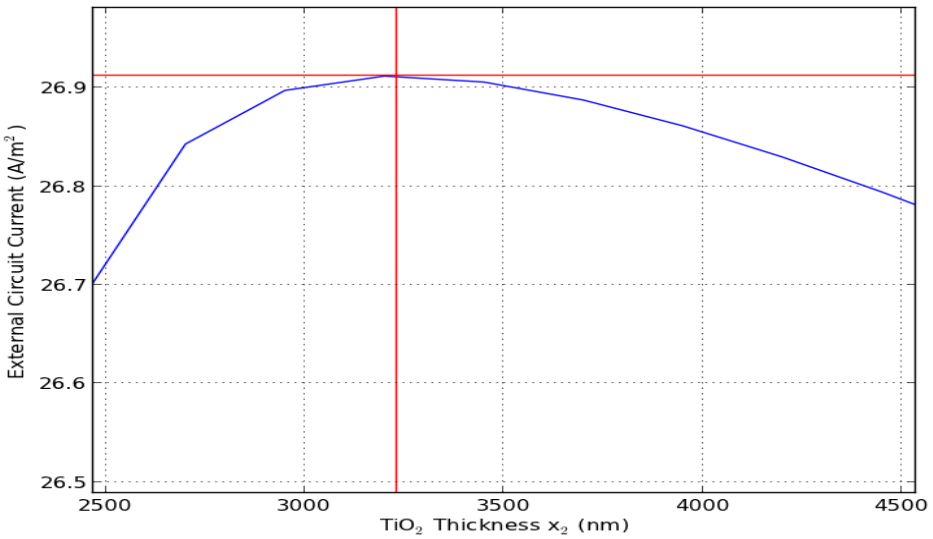


Figure 4.9: A closer look of the optimal conditions

Because of the assumption that each two electrons reaching the cathode will result in the production of a hydrogen molecule $H_2$, the number of moles of hydrogen is optimized by optimizing the external current. The number of moles of hydrogen can be calculated using Eq.(3.20):

$$\begin{aligned} n_{\mathrm{H_2}} &= \frac{I}{2qA_v} \\ &= \frac{26.9 \text{ A/m}^2}{2 \times 1.602 \times 10^{-19} C \times 6.022 \times 10^{23} 1/\text{mole}} \\ &= 1.394 \times 10^{-4} \qquad \text{mol/(m}^2\text{s)} \end{aligned}$$

The volumetric flow rate of $H_2$ gas generated at the cathode can be calculated using the ideal gas low, and so at atmospheric pressure and 298 °K:

$$\begin{aligned} \dot{V}_{H_2} &= \frac{\dot{n}RT}{P} \\ &= \frac{1.394 \times 10^{-4} \text{ mol/s} \times 8.314 \text{ J/(mol K)} \times 298 \text{ K}}{101325 \text{ Pa}} \\ &= 3.41 \times 10^{-6} \qquad \text{m}^3/(\text{m}^2\text{s}) \\ &= 3.41 \qquad\qquad\quad \text{cm}^3/(\text{m}^2\text{s}) \end{aligned}$$

The overall efficiency of the PEC cell is given by Eq.(3.21):

$$\begin{aligned} \eta_c &= \frac{I(1.23 - V_{bias})}{I_r A} \\ &= \frac{26.9(1.23 - 0)}{970 \times 1} \\ &= 3.41\% \end{aligned}$$

The overall efficiency is relatively high compared to the published literature, and it is primarily due to the different nonidealities occurring in the system that we did not capture in the model. At first, the published work may have higher

values of cell components electrical resistances which may decrease the external current, and thus lower the overall cell efficiency. Furthermore, the model did not count for the electrochemical reactions rate modeling, and did not consider the decreased reaction surface area due to hydrogen and oxygen gas bubbles evolving at the electrodes. In addition, $TiO_2$ band edge alignment with the redox potentials were not considered in the model, which may require additional over-potential to allow the redox reactions occurrence. Table 4.2 shows a some of the overall efficiencies achieved in the literature, and it is clear that when using sunlight, the overall efficiencies are small.

Table 4.2: Overall cell efficiency comparison

| Authors | $\eta_c$ % | Light Source |
|---|---|---|
| Fujishima et al. [15] | 0.4 | Sunlight |
| Ghosh et al. [18] | 0.6 | Sunlight |
| Bak et al. [16] | 0.4 | Sunlight |
| Li et al. [34] | 2.6 | UV light |

The model results and parameters are shown in Table 4.3 at the optimum conditions.

Table 4.3: Model results at the optimum conditions.

| $x_1$ (nm) | $x_2$ (nm) | $I^{opt}$ (A/m$^2$) | $H_2$ (mol/(m$^2$s)) |
|---|---|---|---|
| 400 | 3230 | 26.9 | 1.394 $\times 10^{-4}$ |
| $H_2$ (cm$^3$/(m$^2$s)) | $\eta_c$ (%) | $V_{oc}$ (V) | $G_t$ (e\h/m$^2$) |
| 3.41 | 3.41 | 2.75 | 1.82 $\times 10^{20}$ |
| $U^{total}$ (e\h/m$^2$) | $I_{ph}$ (A/m$^2$) | $I_o$ (A/m$^2$) | $R_{ITO}$ ($\Omega$) |
| 2.97 $\times 10^7$ | 29.2 | 7.31 $\times 10^{-46}$ | 0.1 |
| $R_{TiO_2}$ ($\Omega$) | $R_{KOH}$ ($\Omega$) | $R_{Pt}$ ($\Omega$) | $R_s$ ($\Omega$) |
| $2.6\times 10^{-3}$ | $5\times 10^{-5}$ | $10.6\times 10^{-5}$ | 0.1 |

One can notice that the dark current is a very small number; however, it should not be neglected. From Eq.(3.15), $I_o$ is multiplied by the exponential term

$$\begin{aligned}
&\exp\left[\left(q\frac{V-IR_s}{\beta k_B T}\right)-1\right] \\
&= \exp\left[\left(1.602\times 10^{-19}\frac{0-26.9\times 0.1}{1.38\times 10^{-23}\times 298}\right)-1\right] \\
&= 3.1\times 10^{45}
\end{aligned}$$

Therefore, when $I_o$ is multiplied by the exponential number, we will have

$$7.31 \times 10^{-46} \times 3.1 \times 10^{45} = 2.3A$$

Thus, the current $I$ is

$$I = -29.2 + 2.3 = -26.9A$$

The large open circuit voltage ($V_{oc}$ = 2.75 V) and the small dark saturation current ($I_o = 7.31 \times 10^{-46}$) are basically due to large $TiO_2$ bandgap. The PV-EDUCATION website [35] has interesting plots of the open circuit voltage and dark saturation current as functions of band gap, and the $V_{oc}$ and $I_o$ obtained in this research matches the values in the website plots at a band gap of 3.0 eV.

## 4.6 Current Voltage Curve

The current-voltage curve can be obtained using Eq.(3.15) at $TiO_2$ optimum thickness of 3230 nm, and ITO thickness of 400 nm. By changing the voltage in Eq.(3.15), we obtain different current values and so we can plot the I-V curve as in Figures 4.10 and 4.11. Note that the current data obtained from Eq.(3.15) are actually negative for voltage values less than $V_{oc}$, indicating the direction of the conventional current from the cathode to the anode, and electron current from the anode to the cathode. However, Figures 4.10 and 4.11 are plotted with an opposite sign in order to be consistent with the previous figures, where the current is also plotted in the opposite sign.

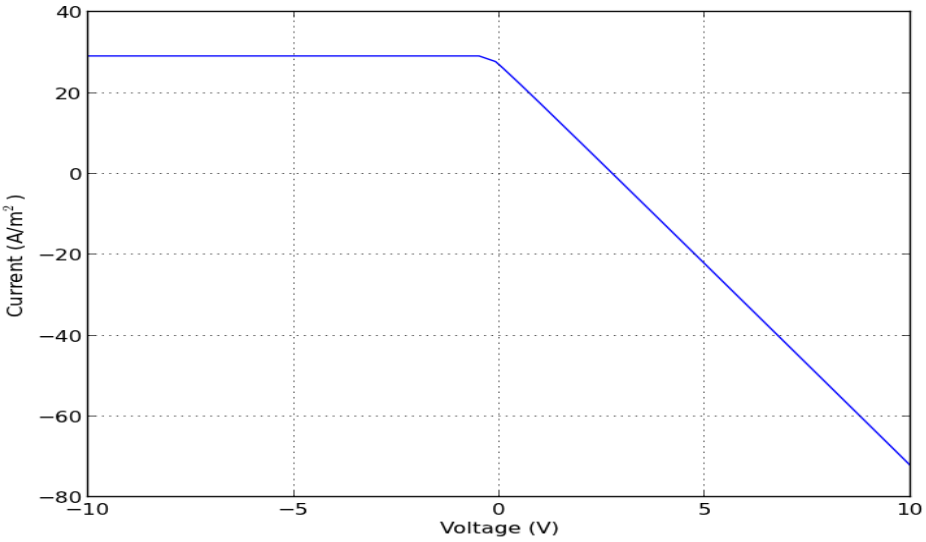


Figure 4.10: Current versus voltage at optimum conditions

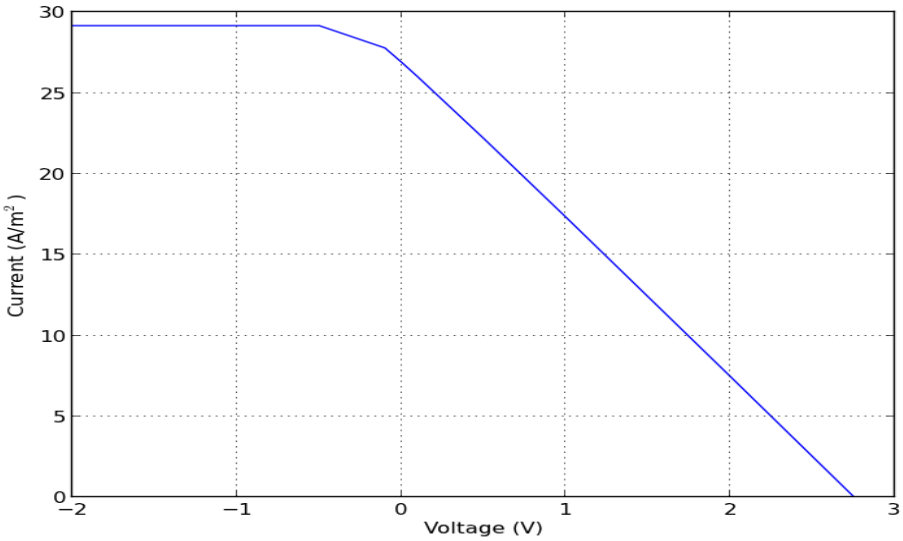


Figure 4.11: A closer look at the I-V curve at optimum conditions

Figure 4.11 shows the optimum current (26.9 $A/m^2$) at short-circuit conditions (V= 0 V), and emphasizes the open-circuit voltage $V_{oc}$ = 2.75 V at I = 0 $A/m^2$. Furthermore, the slope of the curve in the forward bias is 10 which is equal to the inverse of the $R_s$ value. The non-symmetric behavior of the curve in the forward bias and reverse bias indicates the rectifying junction between the $TiO_2$ and the electrolyte [36].

The published current-voltage curves of the PEC cells in the literature can have two behaviors depending on the experimental circuit configuration used. Figure 4.12 shows an experimental circuit diagram where a reference electrode is used, and the voltage obtained and used in the curve is the voltage difference between the reference electrode and the photoanode. Figure 1 in Fujishima et. al. [14] is obtained with an experimental circuit configuration similar to Figure 4.12. On the other hand, Figure 4.13 is an experimental circuit diagram where no reference electrode is used, and the voltage plotted in the current-voltage curve is the voltage difference between the two electrodes. This circuit configuration follows the empirical diode equation and produces a current-voltage curve, which is sometimes referred to as the photovoltaic output characteristics, similar to the one obtained in this thesis. Both Figures 4.12 and 4.13 are recreated from Figure 1 in Sawant et. al. [36].

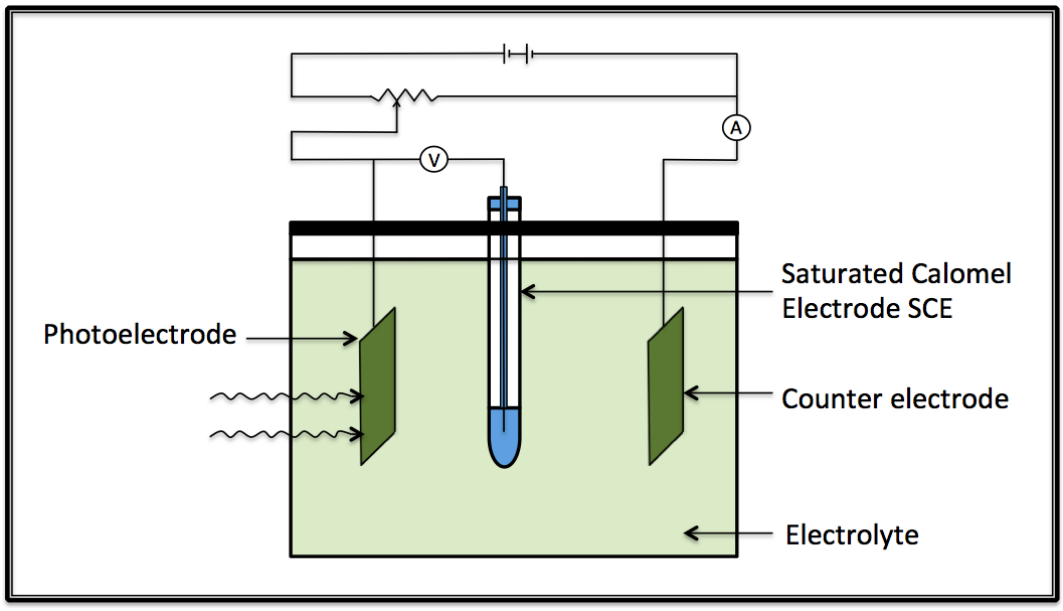


Figure 4.12: Experimental circuit diagram with a reference electrode [36]

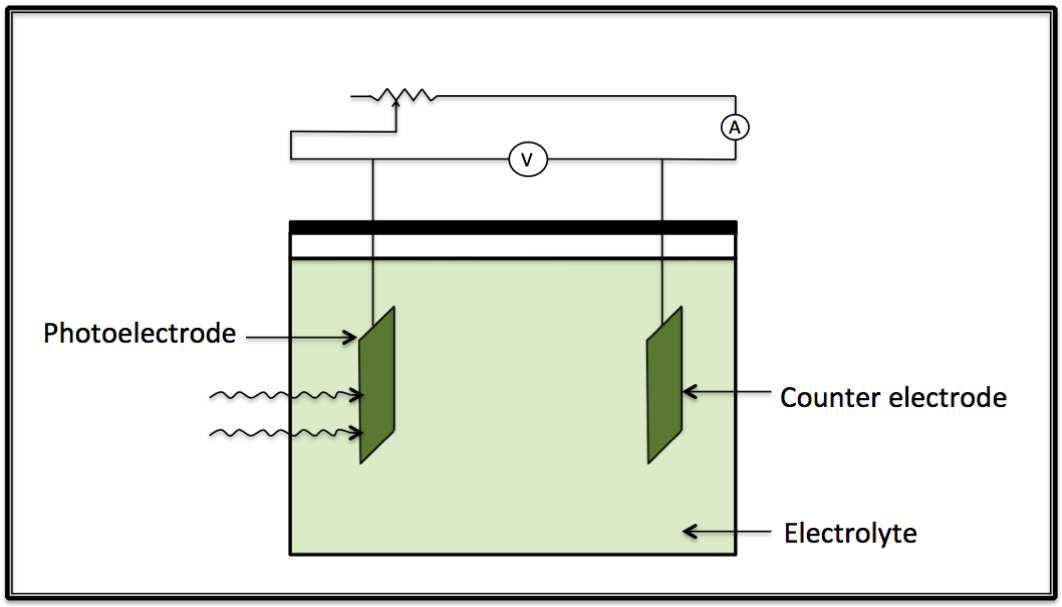


Figure 4.13: Experimental circuit diagram where no reference electrode is used [36]

## 4.7 Concentrated Systems

If a system is designed to have more sunlight concentration, i.e. with a concentration factor $X > 1$, better results will be achieved. The concentration factor $X$ will primarily affect the photocurrent, and slightly affect the open circuit voltage as in Eq.(3.18). The external circuit current equation used for this case will be [6]

$$I = -XI_{ph} + I_o \left[ \exp\left( q\frac{V - IR_s}{\beta k_B T} \right) - 1 \right] \tag{4.7}$$

where $I_{ph}$ represents the photocurrent at $X = 1$, and the term $XI_{ph}$ will represent the increased photocurrent generated by solar concentration. The results might not change that much at ITO thickness of 400 nm, but when we increase the ITO thickness by 50 nm, to be 450 nm, the external current and the hydrogen generation rate are more than doubled as in Table 4.4 and Figure 4.14.

Table 4.4: Optimization results for a concentration factor of $X = 2$.

| $x_1$ nm | $x_2^{opt}$ nm | $I^{opt}$ A/m$^2$ | $H_2$ moles/(m$^2$s) | $H_2$ cm$^3$/(m$^2$s) |
|---|---|---|---|---|
| 400 | 1101 | 28.1 | 1.46 $\times 10^{-4}$ | 3.57 |
| 450 | 4536 | 60.2 | 3.12 $\times 10^{-4}$ | 7.63 |

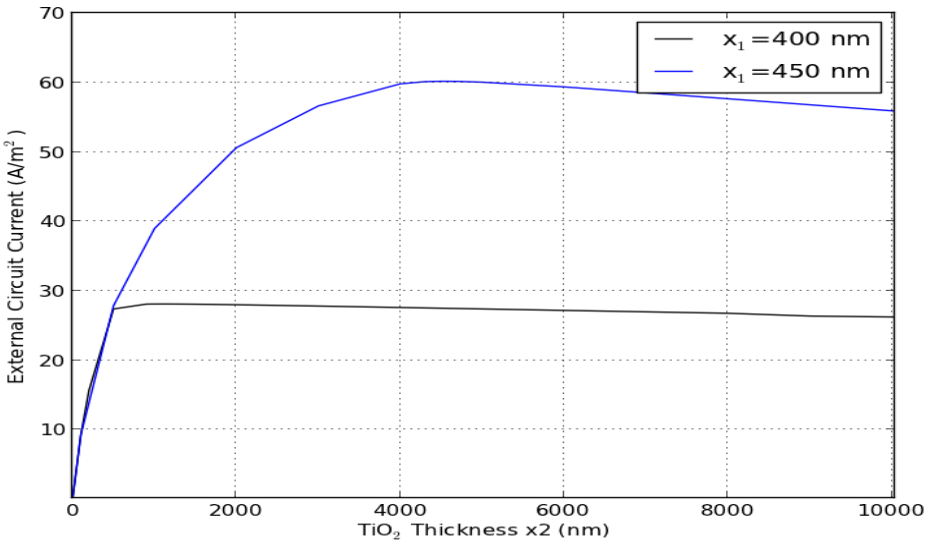


Figure 4.14: External current $I$ at X= 2 as a function of $x_2$

# Chapter 5: Conclusion and Future Work

In this research, a photoelectrochemical cell model is developed, where titanium dioxide ($TiO_2$) is used as a photoanode material, platinum (Pt) as a cathode, and 1 M potassium hydroxide (KOH) solution as an electrolyte. The photoanode consists of a $TiO_2$ film deposited on a quartz ($SiO_2$) substrate coated with indium tin oxide (ITO) as a transparent conducting oxide. Light would travel through $SiO_2$ and ITO before it reaches $TiO_2$, where photons can be absorbed in order to generate electron/hole pair necessary to drive the surface reactions in order to split water to hydrogen and oxygen. The main objective is to maximize the production of hydrogen at the cathode by optimizing the external current, with $TiO_2$ and ITO thicknesses as optimization variables. This research is contributing to the field since the effect of $TiO_2$ and ITO thicknesses on the hydrogen generation rate has not been adequately addressed in the literature. In addition, if another material is used as a photoanode, similar model methodology can be used to find the optimum thickness of the anode films in order to maximize the hydrogen generation rate.

## 5.1 Summary and Conclusions

In this research, the Beer-Lambert law is used in conjunction with the empirical diode equation to calculate the electron/hole pair generated in the photoanode, and the external current reaching the cathode. Several nonidealities were included in the model such as the light reflection between the anode electrode films, and the series resistance represented in ITO, $TiO_2$, KOH, and Pt electrical resistance. The light reflection did not have a substantial effect on the model since its maximum value did not exceed 11%. The electrical resistance of Pt and the KOH solution also did not have a considerable effect due to their low resistivity and assumed thicknesses of 1 mm each. The electrical resistance of $TiO_2$ does not have a significant effect for small values of thickness (up to 3000-3500 nm) since the electron/hole pair generation rate is significantly increasing; however, as the $TiO_2$ thickness increases above 3230 nm, the external current is reduced owing to the increased resistance.

As a reasonable approach, the thickness of ITO was chosen to be 400 nm since there is not an optimum thickness of ITO at which the current is maximized. The optimization results showed an optimum value of the external current of 26.9 $A/m^2$ at $TiO_2$ thickness of 3230 nm. The optimum solution of 3230 nm seems reasonable since the total electron/hole generation rate does not increase enough to overcome the increasing electrical resistance of $TiO_2$ as the thickness increases. At the optimum conditions, the moles of hydrogen generated is 1.394 $\times 10^{-4}$ mol/($m^2$s), with a volumetric flow rate of 3.41 $cm^3/(m^2s)$, and a cell overall efficiency $\eta_c$ = 3.41 %. A concentration factor $X = 2$ was tested to check the effect it has on

the external current. The results showed that the current, and thus the hydrogen production rate, were more than doubled at an ITO thickness of 450 nm and an optimum $TiO_2$ thickness of 4536 nm. At these optimum conditions, the external current is 60.2 $A/m^2$, the moles of hydrogen produced is 3.12 $\times 10^{-4}$ $mol/(m^2s)$, and the volumetric flow rate was 7.63 $cm^3/(m^2s)$.

## 5.2 Implications for Future Research

The work done in this thesis can be extended with different approaches. Some of the assumptions made in the model can be relaxed and more nonidealities can be added to better represent the system. It was assumed that each two electrons reaching the cathode will result in the production of a hydrogen molecule; however, that is not always the case. Electrons can also involve in other side reactions [37] and, thus, accounting for all the possible side reaction is important. In addition, because the redox reactions are surface reactions, an active site has to have an access to electrolyte and electrons. Due to the evolution of oxygen and hydrogen gas at the anode and cathode, the electrode surfaces can be partially covered with gas bubbles reducing the active surface area of the electrode. In addition, the light reflection model did not include the reflection at the glass window of the PEC cell and in the electrolyte as light travels to reach the photoanode; hence, a more sophisticated model would account for these nonidealities. For simplicity purposes, only one type of charge carriers recombination was considered (the radiative recombination); thus, it is important to consider different types of charge carriers recombination, especially

the surface recombination, to make the model more realistic. Another important issue is to focus on the surface reactions mechanism and rate equations, and specify the rate limiting step to improve the reactions rate. One option is to consider a catalyst material at the anode and cathode to lower the reactions activation energy and hence enhance the rate of reaction. Furthermore, investigating $TiO_2$ band edge alignment with the water electrolysis potentials, as shown in T. Bak et al. Figure 13 [2], and the Pt work function, and estimating the position of the equilibrium Fermi-level position after the cell components contact is established are crucial to better understand the system and determine whether extra potential is required to initiate the redox reactions at the electrodes. In addition, a good approach is to extend the work done in this thesis with a follow up experiment to support the results. Another approach is to work on the $TiO_2$ electrode itself by enhancing its electrochemical properties. Lowering the band gap of $TiO_2$ and the search for effective doping materials are good options for research in order to increase the efficiency of the photoelectrochemical process.

# Bibliography


[1] Santos, Diogo M. F., Sequeira, Cesar A. C., and Figueiredo, Jose L. (2013). Hydrogen production by alkaline water electrolysis. *Quimica Nova, 36*(8), 1176-1193.

[2] Bak, T., Nowotny, J., Rekas, M., and Sorrell, C.C. (2002). Photo-electrochemical hydrogen generation from water using solar energy. Materials-related aspects *International Journal of Hydrogen Energy 27*, 991-1022.

[3] Lopes, T., Andrade, L., Ribeiro, H. A., and Mendes, A. (2010). Characterization of photoelectrochemical cells for water splitting by electrochemical impedance spectroscopy. *International Journal of Hydrogen Energy 35* , 11601–11608.

[4] Nie, J., Chen, Y., Boehm, R. F., and Katukota, S. (2010). A Photoelectrochemical model of proton exchange water electrolysis for hydrogen production. *Journal of Heat Transfer 130*.

[5] Grimes, C. A., Varghese, O. K., and Ranjan, S. (2008). *Light, water, hydrogen: the solar generation of hydrogen by water photoelectrolysis*. New York: Springer.

[6] Adomaitis, R. A. (n.d) *Modeling and analysis of photovoltaic and electrochemical solar energy systems*. Unpublished manuscript. Department of Chemical Biomolecular Engineering, University of Maryland, College Park, MD.

[7] National Renewable Energy Laboratory (NREL). *Reference Solar Spectral Irradiance: Air Mass 1.5*. Retrieved from http://rredc.nrel.gov/solar/spectra/am1.5/

[8] Nowotny, M.K., Bogdanoff, P., Dittrich, T., Fiechter, S., Fujishima, A., and Tributsch, H. (2010). Observations of p-type semiconductivity in titanium dioxide at room temperature. *Materials Letters 64* , 928-930.

[9] Nelson, J. (2003) *The physics of solar cells*. London: Imperial College Press.

[10] Huff, H., Gilmer, D. (2005) *High Dielectric Constant Materials: VLSI MOSFET Applications*. Berlin; New York: Springer.

[11] Jones, A. C., and Hitchman, M. L. (2009) *Chemical vapour deposition: precursors, processes and applications, page* (p 456). Cambridge, UK : Royal Society of Chemistry.

[12] Ginley, D., Hosono, H., and Paine, D. C. (2010) *Handbook of transparent conductors*(p 236). New York; London: Springer.

[13] Bott, A. W. (1998). Electrochemistry of semiconductors. *Current Separations 17*(3), 87–91 .

[14] Fojishima, A., and Honda, K. (1972). Electrochemical photolysis of water at a semiconductor electrode. *Nature 238*, 37–38.

[15] Fojishima, A., Kohayakawa, K., and Honda, K. (1972). Hydrogen production under sunlight with an electrochemical photocell. *Journal of Electrochemical Society 122*(11), 1487–1489.

[16] Bak, T., Nowotny, J., Rekas, M., and Sorrell, C.C. (2002). Photo-electrochemical properties of the $TiO_2$-Pt system in aqueous solutions *International Journal of Hydrogen Energy 27*, 1926.

[17] Morisaki, H., Watanabe, T., Iwase, M., and Yazawa, K. (1976) Photoelectrolysis of water with $Ti0_2$-covered solar-cell electrodes *Applied Physics Letters 29*(6), 338340.

[18] Ghosh, A. K., and Maruska, H. P. (1977) Photoelectrolysis of water in sunlight with sensitized semiconductor electrodes *Journal of Electrochemical Society 124*(10), 1516–1522.

[19] Mishra, P.R., Shukla, P.K. and Srivastava, O.N., Comparative photoelectrochemical study of PEC solar cell fabricated with n-$TiO_2$ photoelectrodes at different temperatures and under different oxygen flow rates.

[20] Liang, C.-H., Chang, H.-Y., Liou, T.-W., and Chen, H.-I. (2008). Preparation and characterization of solgel derived $TiO_2$/ITO photoelectrodes. *Surface Review and Letters 15*, 161-168.

[21] Polyanskiy, M. (2008-2014) *Refractive index database*. Retrieved from http://refractiveindex.info

[22] Sigma-Aldrich. *Potassium hydroxide solution*. Retrieved from http://www.sigmaaldrich.com/catalog/product/fluka/00650?lang=enregion=US

[23] Lee, K. D. (2005). Effect of substrate temperature on the optical and the electrochromic properties of sputtered $TiO_2$ thin films. *Journal of the Korean Physical Society 46*(6), 1383–1391.

[24] Marti, A., Luque, A. (2004) *Next generation photovoltaics : high efficiency through full spectrum utilization*(p 54). Bristol; Philadelphia: Institute of Physics.

[25] Krogstrup, P., Jorgensen, H. I., Heiss, M., Demichel, O., Holm, J. V., Aagesen, M., ..., Morral, A. F. (2013). Single-nanowire solar cells beyond the ShockleyQueisser limit. *Nature Photonics 7*, 306–310.

[26] Sigma-Aldrich. *Indium tin oxide coated glass slide, rectangular, surface resistivity 70-100 /sq, slide*. Retrieved from http://www.sigmaaldrich.com/catalog/product/aldrich/576352?lang=enregion=US

[27] Sigma-Aldrich. *Indium tin oxide coated glass slide, rectangular, surface resistivity 30-60 /sq, slide*. Retrieved from http://www.sigmaaldrich.com/catalog/product/aldrich/636908?lang=enregion=US

[28] Sigma-Aldrich. *Indium tin oxide coated glass slide, rectangular, surface resistivity 15-25 /sq, slide*. Retrieved from http://www.sigmaaldrich.com/catalog/product/aldrich/636916?lang=enregion=US

[29] Sigma-Aldrich. *Indium tin oxide coated glass slide, rectangular, surface resistivity 8-12 /sq, slide*. Retrieved from http://www.sigmaaldrich.com/catalog/product/aldrich/578274?lang=enregion=US

[30] Senain, I., Nayan, N., and Saim, H. (2010) . Structural and electrical properties of $TiO_2$ thin film derived from sol-gel method using titanium (IV) butoxide.*International Journal of Integrated Engineering 2*(3), 29–35.

[31] Cadena, R. (2014) *Electricity for the entertainment electrician technician*(p 7). Massachusetts; Oxford: Focal Press.

[32] Gilliam, R.J., Graydon, J. W., Kirk, D. W., and Thorpe, S. J. (2007). A review of specific conductivities of potassium hydroxide solutions for various concentrations and temperatures. *International Journal of Hydrogen Energy 32*, 359364.

[33] Licht, S. (2001). Multiple band gap semiconductor/electrolyte solar energy conversion. *The Journal of Physical Chemistry B 105* 6281-6294.

[34] Li, Y., Yu, H., Song, W., Li, G., Yi B., and Shao, Z. (2011). A novel photoelectrochemical cell with self-organized $TiO_2$ nanotubes as photoanodes for hydrogen generation. *International Journal of Hydrogen Energy 36*, 14374–14380.

[35] Photovoltaic Education Network. *Open-Circuit Voltage*. Retrieved from http://pveducation.org/pvcdrom/solar-cell-operation/open-circuit-voltage

[36] Sawant, R.R., Shinde, S.S., Bhosale, C.H., and Rajpure, K.Y. (2010). Influence of substrates on photoelectrochemical performance of sprayed n-CdIn2S4 electrodes. *Solar Energy 84*, 1208-1215.

[37] Hameed, A., Gondal, M.A., Yamani, Z.H., and Yahya, A.H. (2005). Significance of pH measurements in photocatalytic splitting of water using 355 nm UV laser. *Journal of Molecular Catalysis A: Chemical 227*, 241–246.